2006

Strategic geographic positioning of sea level gauges to aid in early detection of tsunamis in the Intra-Americas sea

Joshua I. Henson
University of South Florida

Strategic geographic positioning of sea level gauges to aid in early detection of tsunamis in the Intra-Americas Sea

by

Joshua I. Henson

A thesis submitted in partial fulfillment
of the requirements for the degree of
Master of Science
College of Marine Science
University of South Florida

Major Professor: Frank Muller-Karger, Ph.D.
Doug Wilson, Ph.D.
Mark Luther, Ph.D.
George Maul, Ph.D.

Date of Approval:
April 6, 2006

Keywords: iocaribe-goos, tsunamigenic risk analysis, numerical modeling, ncom, caribbean

Acknowledgements

Many people have contributed their time and experience to this work. I thank them for their dedication and especially their patience. They are Christine Kranenburg, Carrie Wall, Jesse Lewis, Judd Taylor, Brock Murch, Remy Luerssen, Dr. Chuanmin Hu, Dr. Luis Garcia-Rubio, Dr. Chris Moses, Zhiqiang Chen, Digna Rueda, Dr. Paul Zandbergen, Damaris Torres-Pulliza, Inia Soto, and Laura Lorenzoni. I also thank Vembu Subramanian, Jeff Scudder, Cliff Merz, Rick Cole, and Jay Law for their support and expertise with ocean/met systems. I would especially like to thank Dr. Steve Morey for sharing his knowledge and experience of the NCOM, without which, much of this work would not have been possible. I must also thank my fiancée, Susan, for her support and understanding over the past two years. This work was funded by NOAA grant number EA133R-05-SE-5280.

Note to the reader: The original document contains color which is necessary to fully understand some figures. The original manuscript is on file with the USF library in Tampa, FL.

Table of Contents

List of Tables iii

List of Figures iv

Abstract v

Introduction 1
- Historical Tsunamis in the IAS Region 2
- The Caribbean and Surrounding Tectonic Plates 3
- Tsunamigenic Earthquakes 4
- Tsunamigenic Submarine Slides, Slumps and Landslides 5
- Tsunamigenic Volcanic Events 6
- Sea Level Gauges in the Caribbean and Adjacent Regions 8

Methods 9
- Creation of Tsunamigenic Events List 9
- Determination of IAS Tsunamigenic Potential 16
- Modeling 18
  - Bathymetry 19
  - Initial conditions 19
- Determination of Coastal Grid Points (CGP), Population Data Incorporation, and Time Series Analysis 21
- Sea Level Gauge Location Determination 25
- Location Priority for Coastal Sea Level Gauges 26

Results and Discussion 28
- Modeling Validity 28
- Tsunami Travel Time and IAS Coastline Vulnerability 29
- Sea level Gauge Location Priority 31
- Operational Sea Level Gauges in the Caribbean 33

Conclusions and Recommendations 36

References 38

Bibliography 44

Appendices 46
- Appendix A: A Note on Dry Cell Issues and Bathymetry Alterations 47

Appendix B: Initial Condition and NCOM Parameter Options Experiments 48
Introduction 48
Methods 48
Results and Discussion 49
Surface field output interval 49
Integration time step 49
Initial amplitude and e-folding radius 50
Seafloor roughness 51
Total run time 51
Appendix C: Travel Time Post Processing Experiments 52
Introduction 52
Methods and Discussion 52
Appendix D: Isochron / NCOM Travel Time Comparison Tests 56
Introduction 56
Methods 56
Results and Discussion 57
Appendix E: Travel Time Verification Study 58
Introduction 58
Results and Discussion 58
Aguadilla 58
Mayagüez 58
Boqueron 59
Conclusion 60

List of Tables

Table 1.	List of modeled events, ordered chronologically	11
Table 2.	Weight assignments to the tsunamigenic event source map	16
Table 3.	Sensitivity test results summary	20
Table 4.	List of population and tourist centers	23
Table 5.	Decision rank matrix	32
Table 6.	List of initial sea level gauge locations recommend for a tsunami warning system	32
Table B1.	Time series analysis locations	48
Table B2.	Values used in sensitivity experiments 1-10	48

List of Figures

Figure 1.	Plate boundaries and tsunamigenic source regions	4
Figure 2.	The locations of the 42 historical tsunamis simulated in this study	10
Figure 3.	1-degree resolution grid, map of the IAS, historical tsunami origins, and tsunamigenic source regions	17
Figure 4.	Sector total weights	17
Figure 5a.	All 10,623 coastal grid points used in the initial time series analysis study	22
Figure 5b.	Inset of figure 5A; Close-up view of CGPs around Puerto Rico	22
Figure 6.	8,009 CGP's with attributed population data	23
Figure 7.	Population and tourist centers	24
Figure 8.	Top 5% of risk sectors	26
Figure 9.	Impact frequency	30
Figure 10.	Mean travel time	30
Figure 11.	Median travel time	31
Figure 12a.	Operational and recommended sea level gauge stations in the IAS	34
Figure 12b.	Inset of figure 12a; Close-up view of stations around PR, the USVI, and the Dominican Republic	35
Figure C1.	Surface elevation time series at Krum Bay, USVI resulting from the 1918 Puerto Rico tsunami	52
Figure C2.	Surface elevation time series at a generic point resulting from the 1918 Puerto Rico tsunami	54
Figure D1.	Sector I30 isochrones	56
Figure E1.	Sea level time series at Aguadilla resulting from the 1918 Puerto Rico Tsunami	58
Figure E2.	Sea level time series at Mayagüez resulting from the 1918 Puerto Rico Tsunami	59
Figure E3.	Sea level time series at just east of Mayagüez, in the bay of Mayagüez resulting from the 1918 Puerto Rico Tsunami	59
Figure E4.	Sea level time series at Boqueron resulting from the 1918 Puerto Rico Tsunami	60

Strategic geographic positioning of sea level gauges to aid in early detection of tsunamis in the Intra-Americas Sea

Joshua I. Henson

ABSTRACT

A tsunami is a series of large amplitude, shallow water waves generated by an event capable of displacing a massive volume of water. The displaced water propagates at speeds in excess of 800 kph until it dissipates or impacts a shoreline where it slows to 30 – 50 kph [*NOAA and USGS Fact Sheet*, 2005]. Earthquakes are the predominant tsunamigenic event, however, landslides, avalanches, submarine slumps or slides, volcanic eruptions, volcano flank failure, and meteor impact into an ocean can also cause a tsunami [*McCann*, 2004; *O'Loughlin and Lander*, 2003; *Pararas-Carayannis*, 2004]. This study includes past Caribbean tsunamigenic events assumed to be regionally destructive and generated by earthquakes and/or massive submarine slides/slumps. The approximate study area is from 7ºN, 59ºW to 36ºN, 98º W. Caribbean tsunami data suggests that a tsunami will occur in this region once every three years, and destructively once every 21 years [*O'Loughlin and Lander*, 2003]. Excluding the December 2004 Indian Ocean tsunami, approximately 13.8% of all tsunamis and 83% of all tsunami fatalities worldwide have occurred in the Caribbean [*O'Loughlin and Lander*, 2003]. In the past 150 years, 2,590 victims died from tsunamis in the Caribbean. As a result of these recorded fatalities and the rise of Caribbean population by almost 300% from 1950 to 2000 [*CIAT et al*., 2005], protection of human life is a primary reason for establishing a tsunami warning system in this region. The goal of this study is to identify the minimum number of sea level gauge locations to aid in tsunami detection in order to provide the most warning time to the largest number of people. This study defines which historical tsunamis were likely to have been regionally destructive, analyzes the tsunamigenic potential and population distribution of the Intra-Americas Sea (IAS), models 42 historical tsunamis with the United States Navy Coastal Ocean Model (NCOM), and recommends 12 prioritized locations for coastal sea level gauge installation. The results of this systematic approach to assess priority locations for coastal sea level gauges will assist in developing a tsunami warning system for the IAS and are currently being used by NOAA and IOCARIBE-GOOS.

INTRODUCTION

A tsunami is a series of large amplitude, shallow water waves generated by an event capable of displacing a huge volume of water. Whether a wave is considered to be a shallow or deep water wave depends on its wavelength and the depth of water. Deep and shallow-water waves are defined by the ratio of their wavelength to the water depth.

Deep-water wave: $\lambda < 2\ z$
Shallow-water wave: $\lambda > 20\ z$
where, λ = wavelength and z = water depth

While tsunamis are usually generated in deep water, they are considered shallow-water waves because a typical wavelength of a tsunami is 220 km and the average depth of the Caribbean is approximately 2.6 km.

Tsunamis can propagate at phase speeds in excess of 800 kph until they dissipate or encounter shallow water where they slow to 30 – 50 kph [*NOAA and USGS Fact Sheet*, 2005]. Tsunami dissipation primarily depends on the magnitude and character of the tsunamigenic event, although bathymetry and bottom type must also be considered. Eventually, the tsunami is likely to impact a shoreline where life and property are in harm's way. This study seeks to understand how and where tsunamis are generated, how they travel throughout the Caribbean and adjacent regions, and where a minimum number of sensors should be located to most efficiently warn the public of an impending tsunami.

In order to produce a warning, a system must be in place to first detect the wave and predict potential impact locations and severity. Different types of tsunami warning systems/networks are currently being successfully employed to measure, record, and telemeter both oceanographic and meteorological data. Standard means of telemetry include satellite, radio, cellular, telephone line, or Internet. One type of tsunami monitoring system involves Real-Time Kinematic Global Positioning System (RTK-GPS) technology [*Kato, et al.*, 2001]. Curtis [2001] suggests a multi-sensor approach. The Pacific Tsunami Warning System utilizes a combination of coastal sea level gauges and Deep-ocean Assessment and Reporting of Tsunamis (DART) buoys to acquire data for tsunami detection and propagation/run-up prediction. Wave data is captured and telemetered to a base station and input to a model. The model then predicts locations the tsunami is likely to impact.

The predominant tsunamigenic events are earthquakes; however landslides, avalanches, submarine slumps or slides, volcanic eruptions, volcano flank failure, and oceanic meteor impact can also cause a tsunami [*Lander, et al.*, 2002; *McCann*, 2004; *Pararas-Carayannis*, 2004]. Often, a tsunami is the result of coinciding events, thus it can be difficult to identify the tsunamigenic source. Seismic and/or volcanic activity can produce a submarine landslide, which can in turn generate a tsunami. When analyzing events from pre-instrument periods it can be difficult to determine if a submarine slump

or slide occurred and the actual direct tsunamigenic event, such as this, may have gone undetected.

The manner in which a tsunami is generated will affect the warning time available [*Lander, et al.*, 1999]. This warning time can be maximized by predicting how and where the next Intra-Americas Sea (IAS) tsunami is most likely to occur. In general, the closer a sea level gauge is to a tsunami origin the more warning time available.

When designing a tsunami warning system it is critical to understand the types of tsunamigenic mechanisms, the coastlines that are more likely to be affected by a tsunami, tsunami travel time to those coasts, and the resulting effects from historical tsunamis [*Lander, et al.*, 1999]. However, the historical record is incomplete. Therefore, this study aims to define what historical tsunamis were likely to have been regionally destructive by simulating tsunamigenic events with the potential to have far-field (greater than 1000 km) destructive consequences and illustrating where impacts were possible. These efforts are used, in conjunction with IAS population data, to determine the most critical and advantageous locations for the installation of coastal sea level gauges.

Discussed later, most sub-aerial landslides and volcanic tsunami origins are only locally destructive and are therefore not considered in this study. In order to determine if a tsunami is truly destructive at a location, high resolution bathymetry and a model with run-up capability is required to predict the extent of inundation. Wave height along the coast is not analyzed in this study because local effects dictate the necessity of very high bathymetric and model grid resolution to determine wave amplitude at the seashore. Run-up results along a coastline can vary by a factor of 10 [*Hwang and Lin*, 1969; *Smith and Shepherd*, 1994].

Historical Tsunamis in the IAS Region

Excluding the December 2004 Indian Ocean tsunami, approximately 13.8% of all tsunamis and 83% of all tsunami fatalities worldwide have occurred in the Caribbean [*O'Loughlin and Lander*, 2003]. Caribbean tsunami data over the past 100 years suggests that a tsunami will occur in this region once every three years and destructively every 21 years [*O'Loughlin and Lander*, 2003].

Shallow earthquakes, magnitude 6.5 or greater, cause the majority of Caribbean tsunamis [*McCann*, 2004]. O'Loughlin and Lander [2003] describe 127 reported tsunamis in the Caribbean basin over approximately the past 500 years. Of those reported, the authors find that 53 are almost certainly true tsunamis and another 8 are most likely true. These tsunami events were generated by various sources including but not limited to earthquakes, submarine slides/slumps, volcanic eruptions, and more likely a combination of those three. Understanding how past tsunamis have affected the region will help determine how future tsunami disasters can be mitigated.

The historical record of tsunami origins and affected areas is sparse. The data used in this study is taken from both O'Loughlin and Lander [2003] and the National Geodetic Data Center [*NGDC*, 2005]. These original tsunami origin data have 0.1 degree precision [*Dunbar*, 2005, personal correspondence], and while there are historical records of areas affected by some of these events, for others there is no information on effects or arrival location.

Here, a numerical model is used to simulate historical tsunamis. The criteria used to select events that are simulated are discussed under Methods ("Creation of tsunamigenic events list"). The simulations are performed with the U.S. Navy Coastal Ocean Model (NCOM), discussed under Methods ("Modeling").

The Caribbean and Surrounding Tectonic Plates

Tectonic activity due to plate movement is the principal cause of earthquakes, 80% of which occur along the plate boundaries in the oceanic crust [*Woods Hole*, 2005]. In order to fully understand the nature of the earthquakes that may generate tsunamis, the plate boundaries and their movement must also be understood. Figure 1 shows the plates in the region, their boundaries, and summarizes their interactions. The Caribbean (CA) plate is bordered to the north and east by the North American (NA) and South American (SA) plates, to the south by the SA, North Andes (ND), Panama (PM), and Cocos (CO) plates, and to the west by the CO plate [*Bird*, 2003; *Lander, et al.*, 2002; *McCann*, 2004; *O'Loughlin and Lander*, 2003; *Pararas-Carayannis*, 2004]. Sitting on the CA plate are the islands of Hispaniola, Puerto Rico, and Jamaica to the north, the Lesser Antilles to the east, and to the west is Central America. The South American continent boarders the CA plate to the south [*Bird*, 2003; *McCann*, 2004].

The CA plate is moving eastward approximately 20 ± 3 mm/yr relative to the NA and SA plates [*Demets*, 1993; *Grindlay, et al.*, 2005; *Lander, et al.*, 2002; *McCann*, 2004; *O'Loughlin and Lander*, 2003; *Pararas-Carayannis*, 2004; *ten Brink, et al.*, 2004]. Some estimates are as high as 37mm/yr [*Mercado and McCann*, 1998; *Sykes, et al.*, 1982]. The NA and SA plates are subducting under the eastern margin of the CA plate, leading to the formation of the Lesser Antilles volcanic arc. At the northern boundaries, the CA plate is sliding past the NA plate leading to transpressional motion (compressive loading as a result of shear stresses) and uneven or oblique subduction near Puerto Rico [*Lander, et al.*, 2002; *McCann*, 2004; *O'Loughlin and Lander*, 2003]. The southern boundary is characterized by a complex convergent margin near Venezuela and strike-slip faults on land [*McCann*, 2004]. The CO plate is subducting under the CA plate on the western boundary, which also forms a chain of volcanic activity [*Lander, et al.*, 2002]. Further explanation on the tectonic regime of the CA and adjacent plates can be found in McCann [2004] and Grindlay et al. [2005].

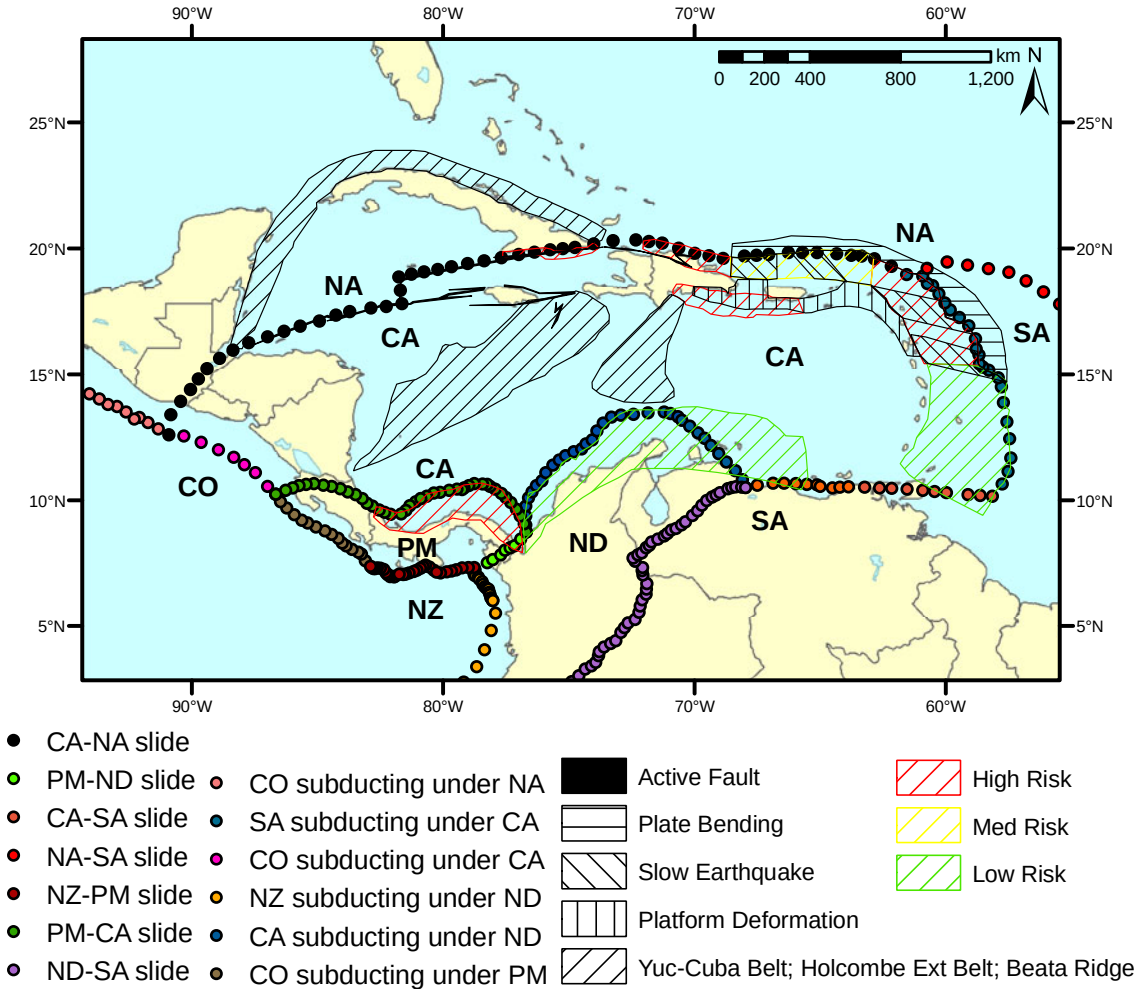

Figure 1 – Plate boundaries and tsunamigenic source regions. This figure is a composite of two datasets. Bird [2003] consists of the plate boundaries and between plate interaction represented by the plate labels and colored dots as shown in the legend. McCann [2004] illustrates areas of tsunamigenic sources.

Tsunamigenic Earthquakes

The nature in which a tsunamigenic earthquake occurs will dictate the attributes of a resulting tsunami. There is a range of possible outcomes due to seismic activity in the Caribbean, some of which are more likely to produce a tsunami [*Grindlay, et al.*, 2005; *McCann*, 2004; *Mercado and McCann*, 1998]. Typically, significant vertical deformation of the sea floor (i.e. a dip/slip earthquake) is required for tsunami generation. This deformation can be due to either isostatic rebound of an accretionary prism near a subduction zone or a change in crustal elevation [*McCann*, 2004; *Okal, et al.*, 2003]. The direction of movement, depth of deformation, length and width of the deforming fault or plate boundary, deformation dip and slip angles, and focal depth will determine the size of the tsunami [*McCann*, 2004; *Polet and Kanamori*, 2000; *Zahibo, et al.*, 2003a]. For example, a shallow subduction zone earthquake or an earthquake with a more vertical angle of deformation will usually displace a larger volume of water and consequently

generate a larger tsunami [*Bilek and Lay*, 2002; *Polet and Kanamori*, 2000]. The overlying geology also determines whether a tsunami will result from an earthquake [*Bilek and Lay*, 2002; *Kanamori*, 1972]. There may be stronger motion at the sea floor than the measured seismic moment would typically represent if a rupture occurs within a sedimentary wedge or the rupture velocity is slow [*Okal, et al.*, 2003; *Polet and Kanamori*, 2000].

Regions where there is potential for an earthquake with a slow rupture velocity, or slow earthquake, to occur have a higher potential to produce tsunami larger than a seismometer would otherwise indicate [*Polet and Kanamori*, 2000; *Todorovska and Trifunac*, 2001]. When the sea floor deformation velocity is on the same order as tsunami velocity (i.e. a slow earthquake, slide, or slump) the tsunami may be amplified by an order of magnitude [*Todorovska and Trifunac*, 2001]. The amplification may be caused by constructive interference as the tsunami is produced since a slow rupture velocity will yield a longer duration earthquake [*Bilek and Lay*, 2002]. McCann [2004] defines seismic tsunamigenic threats in the Caribbean (see Figure 1) into the following categories: platform deformation, plate bending, slow earthquake, belts and ridges, active faults, and low to high tsunamigenic risk. These regions are based on the geologic and tectonic regime of the IAS. Note how the plate boundaries/interactions [*Bird*, 2003] coincide with the tsunamigenic zones [*McCann*, 2004].

Tsunamigenic Submarine Slides, Slumps and Landslides

A landslide is very similar to a submarine slide or slump, except that falling debris from a landslide begins above the surface of the water. A submarine slide or slump is a gravity driven mass movement of marine sediment and rocks. Sediments that have accumulated on a slope may become unstable and slide down. As the debris flows down it displaces the water in front of it. The volume of water displaced is equal to the volume of sliding debris. Therefore, if the volume of land is known, the amount of displaced water can be determined and from this information wave weight, period, wavelength, and velocity can be calculated.

These types of tsunamigenic events are typically initiated by an earthquake, hurricane or volcanic event such as an eruption or flank failure but may also be initiated without an apparent catalyst [*Jiang and LeBlond*, 1992; *Lander, et al.*, 1999; *McCann*, 2004; *O'Loughlin and Lander*, 2003; *Pararas-Carayannis*, 2004; *von Huene, et al.*, 1989; *Watts and Grilli*, 2004 (Submitted)]. Therefore, it may be difficult to determine whether a slide or an earthquake is the source of a tsunami. For example, the tsunami can be caused by a slide or slump that may or may not be related to an earthquake. In the former case the slide or slump is the secondary tsunamigenic event, while in the latter it is the primary tsunamigenic event. A dip/slip earthquake, as described in the previous section, can produce a tsunami whether or not a slide or slump occurs. Many tsunamis have been generated in areas of the Caribbean where strike/slip plate movement dominates the tectonic activity [*McCann*, 2004]. This suggests a slide or slump as either the primary or secondary tsunamigenic mechanism because vertical deformation of the sea floor is not typically associated with strike/slip plate movement. Through mapping, Grindlay et al. [2005] shows historic evidence of massive slumps or slides along the northern Puerto

Rico margin which most likely generated tsunamis and cracking on the eastern edge of the Mona rift that may lead to the same mass failures as have happened in the past.

Understanding how a tsunami forms helps determine their propagation and destructive potential. Another characteristic of a slide or slump tsunami is their shorter period [*Fryer and Watts*, 2000; *Fryer, et al.*, 2001; *Watts, et al.*, 2003]. In many of these cases, using evidence such as severed or damaged cables, which typically result from a submarine slide or slump, will help determine exactly how a tsunami formed [*Grilli and Watts*, 2005; *McCann*, 2004; *Watts, et al.*, 2003]. Other parameters that influence the occurrence of a slide or slump include bottom type and slope steepness [*McCann*, 2004]. Watts and Grilli [2004 (Submitted)] developed an equation to determine the potential amplitude of a tsunami based on initial slide thickness, initial slide length, mean slide depth, and the mean incline angle. From the Watts and Grilli [2004 (Submitted)] equation, McCann [2004] produced a map illustrating the tsunamigenic potential for every possible slump or slide in the Caribbean. This map shows that every coastline along the strike/slip margin in the west is a potential site for a slide or slump induced tsunami. However, since slide or slump tsunami-like waves have a much shorter period than a typical tsunami, they dissipate faster and are typically only locally dangerous [*Pararas-Carayannis*, 2004]. Therefore, unless the slump or slide is massive, it is unlikely to be regionally destructive. Without detailed ocean bottom mapping and analysis it is difficult to determine the potential for a massive slide or slump. Hence, the slide or slump tsunamigenic potential map of the IAS is not considered in this work.

Tsunamigenic Volcanic Events

The subducting NA and SA plates melt progressively under the CA plate with increasing depth as pressure and temperature rises. As this material heats up, density decreases and the material will tend to rise toward the surface again. This causes an increase in pressure on the crust that lies above, leading to the formation of the Lesser Antilles volcanic arc [*Martin-Kaye*, 1969; *Pararas-Carayannis*, 2004]. Volcanoes along the Lesser Antilles chain are the most likely source for volcanic tsunamigenic events in the Caribbean Sea.

Overall, approximately 5% of tsunamis are volcanic in origin [*O'Loughlin and Lander*, 2003; *Sigurdsson*, 1996]. There are many different volcanic tsunamigenic mechanisms from eruption to structural failure. O'Loughlin and Lander [2003] and Pararas-Carayannis [2004] review case studies of such events, which generated tsunamis that affected Montserrat, Martinique, St. Vincent, and Grenada. These waves originated from the Soufriere Hills volcano on Montserrat Island, the Mt. Pelèe volcano on Martinique, the La Soufrière volcano on St. Vincent, and Kick'em Jenny, a submarine volcano north of Grenada, respectively.

Energy from volcanoes can be transferred to the sea via three main mechanisms: explosions (rapid expansion of gas or other fluids by thermal energy), seawater displaced due to pyroclastic flow reaching the sea (kinetic energy), and collapse of a caldera (potential energy) [*O'Loughlin and Lander*, 2003; *Sigurdsson*, 1996]. Each volcano has individual characteristics that can produce a tsunami and dictates the attributes of the generated wave. The parameters discussed by Pararas-Carayannis [2004] include

geochemical, volcanic explosivity and blast geometry factors, blast orientation and mechanism, and growth and collapses of lava domes.

The tsunami of 26 December 1997 was most likely caused by a landslide triggered by an eruption of the Soufriere Hills volcano on Montserrat [*Heinrich, et al.*, 2001; *Heinrich, et al.*, 1999a; *Heinrich, et al.*, 1998; *Heinrich, et al.*, 1999b; *Pararas-Carayannis*, 2004]. This event resulted in a wave that impacted regions approximately 10 km away, flooding areas at distances of about 80 m inland with a run-up of approximately 3 m [*Heinrich, et al.*, 2001; *Heinrich, et al.*, 1999a; *Heinrich, et al.*, 1998; *Heinrich, et al.*, 1999b; *Pararas-Carayannis*, 2004].

Pararas-Carayannis [2004] also discusses Kick'em Jenny, an active submarine volcano located approximately 8 km north of Grenada. He reports that one tsunami-type wave generated by this volcano had approximately 2 m wave heights observed at the northern coast of Grenada but its effects were not felt in Barbados. He goes on to explain in detail what factors predispose a volcano (both sub-aerial and submarine) to tsunami generation and illustrates the resulting tsunami characteristics. His findings indicate that:

i. Landslides usually only create local tsunamis.
ii. An eruption as large as 20 kilotons will not cause a destructive tsunami since this energy does not translate efficiently to water waves [*Gisler, et al.*, 2004].
iii. Small tsunami-like waves may be generated by a submarine dome collapse.
iv. Currently, the most destructive tsunami that could be created by Kick'em Jenny would cause a maximum run-up of 3 m on the northern coast of Grenada and 1 to 2 m along the western coasts of Barbados, Trinidad, and St. Vincent. These waves would have a period of 1 – 4 min.
v. Tsunamis of volcanic origin can be predicted in advance because volcanic activity is understood, monitored, and renders warning signs prior to eruption or flank failure.
vi. Volcanic tsunamigenic events are not a significant basin-wide threat; however, they are locally dangerous. Specifically this applies to the Soufriere Hills, Mt. Pelèe, La Soufrière, and Kick'em Jenny volcano.

Smith and Shepherd [1993] also modeled a Kick'em Jenny eruption and the results were different from those of Gisler et al. [2004] and Pararas-Carayannis [2004]. Smith and Shepherd [1993] found that the thermal energy reservoir can yield large bubble expansion with an efficient energy yield. Based on this work, Sigurdsson [1996] observed that a Krakatoa magnitude eruption occurring at Kick'em Jenny can lead to a run-up height of 40 m at Grenada and 7 m in the Virgin Islands [*O'Loughlin and Lander*, 2003; *Smith and Shepherd*, 1994]. However, it was later found that more likely to occur is an eruption that would yield a run-up of 8 m at Grenada and 1 m in the Virgin Islands [*O'Loughlin and Lander*, 2003; *Smith and Shepherd*, 1995]. In the event that a destructive tsunami is generated by Kick'em Jenny, its path and dispersal through the Caribbean region is more predictable than the behavior of a seismic tsunamigenic event because the volcano is well instrumented, the number of tsunamigenic parameters is limited, and the point of origin is relatively fixed. The Seismic Research Unit of the University of the West Indies in Trinidad currently monitors the volcano for activity (http://www.uwiseismic.com/KeJ/kejhome.html), but to date there is no tool that

emergency response managers can use to predict the generation or dispersal of a tsunami. Nonetheless, most tsunamis of volcanic origin have relatively local destructive effects and/or are predictable. This limits how useful a basin wide tsunami warning system will be to protect the public from volcanic tsunamigenic events. The best defense against local tsunamis is public education. Therefore, these events will not be considered in this study.

Sea Level Gauges in the Caribbean and Adjacent Regions

Approximately 60 sea level gauge stations were installed in the Caribbean and surrounding countries by NOAA (National Oceanic and Atmospheric Administration), programs such as RONMAC (Water Level Observation Network for Latin America) and CPACC (Caribbean Planning for Adaptation to Global Climate Change), and other locally and internationally funded programs to examine local sea level changes. Government organizations, educational institutions, and independent companies maintain these stations. As of February 2006, the stations were in various states of disrepair, the majority no longer collecting data, and in many cases installations are missing equipment. To contribute to a tsunami warning network, most stations will need to be replaced, while others simply need additional hardware such as a GPS card and/or GOES transmitter [*Henson and Wilson*, 2005].

The IAS Tsunami Warning System (TWS) (IOC UNESCO, 2005) proposal recommends integration of an infrastructure including 31 upgraded sea level stations throughout the wider Caribbean Sea. As of February 2006, out of the 60 stations that had been deployed historically throughout the IAS region, 17 are fully operational and transmitting data, 16 are not operational but the equipment is accounted for, and 10 are questionably operational. The remaining are either no longer operational or not physically there [*Air-Sea Monitoring Systems*, 2006; *Henson and Wilson*, 2005].

Puerto Rico has been aggressively pursuing the development of a tsunami-ready sea level gauge network. The Puerto Rico Seismic Network (PRSN) have begun installing 10 sea level gauge stations around the island and one base station in Mayagüez [*von Hillebrandt-Andrade*, 2006, personal correspondence]. The base station will be capable of processing data from these and other sea level stations throughout the IAS.

METHODS

This study seeks to determine where the minimum number of sea level gauges should be located to maximize the warning time to the largest amount of people. This is achieved by analyzing how and where regionally destructive tsunamis form, propagate, and impact a coastline as well as evaluating the coastal population distribution. It is also essential to know where coastal sea level gauges are operational so monitoring efforts are not duplicated.

Although this study does not intend to pinpoint an origin location, it examines areas where a tsunami is more likely to occur by using a tsunamigenic event source map [*McCann*, 2004] and the origins of 42 historical tsunamis. This risk analysis is critical to maximizing warning time because a sea level gauge should be installed closest to a tsunami origin. Propagation, travel time, and impact analysis is accomplished through the simulation of the historical tsunamis with the NCOM. There are several sub-studies involved in using the NCOM including parameter sensitivity and initial condition analyses and travel time calculations. The amount of warning time available is derived from a combination of modeling with the NCOM, developing isochrones, and estimating travel time to coastal population centers throughout the region. The isochrones are developed independently and then tested against the NCOM results.

The tsunamigenic risk analysis uses a one-degree resolution grid whereas the NCOM uses a 2 arc-min resolution grid. These are two independent studies in that the former is used to determine where the next tsunami is most likely to occur and the latter is used to understand tsunami propagation and travel time. Accuracy, resolution, and precision are not transferable from one grid to the other.

Creation of Tsunamigenic Events List

A total of 61 tsunamis have affected the IAS region in the past 500 years. Event data is taken from both O'Loughlin and Lander [2003] and the NGDC tsunami database [2005]. Since most volcanic and shore based landslide tsunamigenic events have localized effects, they are omitted from this study [*O'Loughlin and Lander*, 2003; *Pararas-Carayannis*, 2004; *Smith and Shepherd*, 1995]. Events are also discarded if the origin is located inland, the origin latitude and longitude cannot be found, or the event did not originate in the IAS.

Each event is rated on a scale of 0 – 4 by the source authors [*NGDC*, 2005; *O'Loughlin and Lander*, 2003] according to the validity of the historical observations. These ratings are derived in different ways, are qualitative, and can be subject to opinion. The validity rating from the two datasets are compared and the higher rating is used. In an effort to create the largest list of probable events, the 42 simulated historical events have a validity rating of 3 or higher. All simulated tsunamigenic sources are assumed to be regionally destructive such as a dip/slip earthquake or massive underwater slump/slide whether caused by an earthquake or not.

It is necessary to adjust some of the historical origin coordinates to properly initialize the NCOM. Where possible, the origin is moved closer to or along a plate boundary, but in some cases they are moved perpendicular to isobaths. Figure 2 shows the origins of the simulated tsunamis based on historical information. The locations reflect adjusted origins. Table 1 provides a list of the events that are modeled and notes which origins are adjusted.

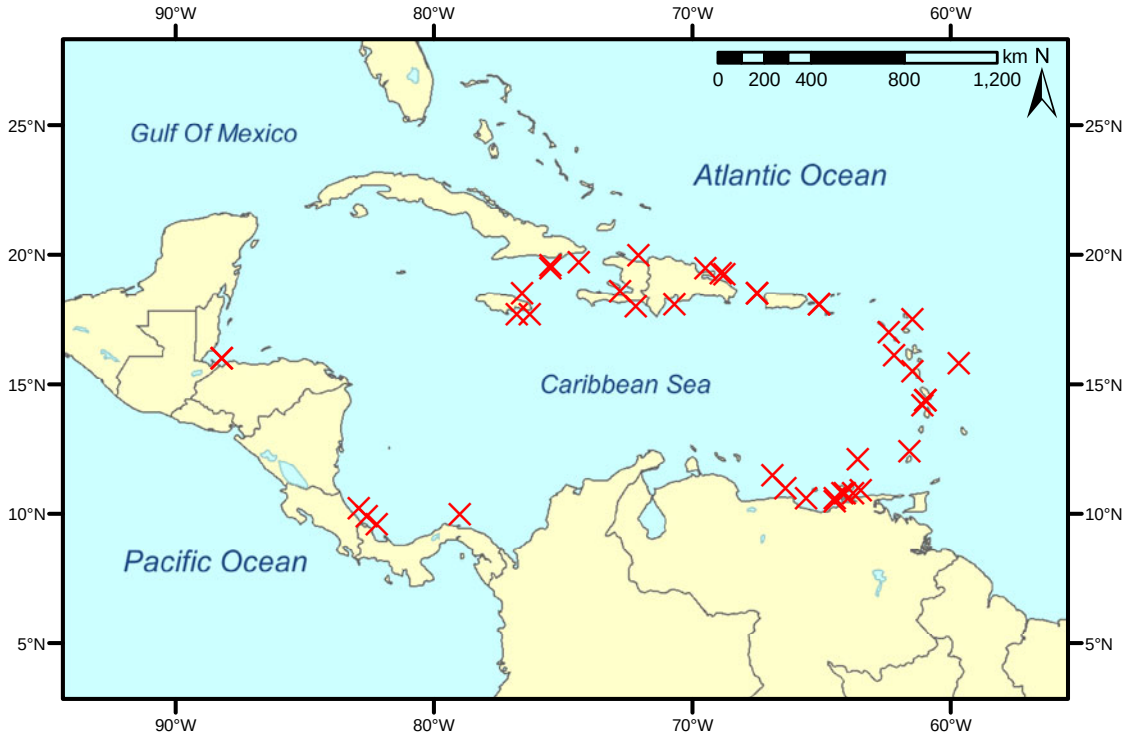

Figure 2 – The locations of the 42 historical tsunamis simulated in this study. The origin of the tsunamigenic events are represented by an "X" (see Table 1). Note that some events have originated in the same location.

Table 1 – List of modeled events, ordered chronologically (see also Figure 2). Shaded cells denote events whose origin is adjusted. The latitude and longitude listed reflect the adjusted location. Where applicable, original coordinates are in parenthesis. Sources: O'Loughlin and Lander [2003] and the NGDC Tsunami Database [2005]. No information was found for cells that are blank.

Tsunami Origin	**Latitude (N)**	**Longitude (E)**	**Date**	**Time**	**Validity rating**	**Earthquake magnitude and corresponding scale**	**Source type and brief description**
Venezuela	10.80 (10.70)	-64.20 (-64.20)	9/1/1530	1430 UT	4		Earthquake
S. Belize	16.00 (16.20)	-88.20 (-88.50)	11/24/1539	2300 LT	4		Earthquake
Venezuela	10.80 (10.70)	-64.10 (-64.10)	9/1/1543	2300 LT	4		Earthquake
Leeward Is.	17.50	-61.50	4/16/1690		4	Ms 8.0	Earthquake; dispute regarding exact day, found 4/06/1690 as well
Jamaica	17.70 (17.90)	-76.80 (-76.90)	6/7/1692	1643 UT	4	Ms 7.5	Earthquake induced submarine landslide
Venezuela	10.60 (10.60)	-64.50 (-64.30)	1726		3		Earthquake
Venezuela	10.50 (10.50)	-64.50 (-64.30)	1750		3		Earthquake
Hispaniola	18.10 (18.30)	-70.70 (-70.70)	10/18/1751	1900 UT	4	Ms 7.3	Earthquake
Haiti	18.00 (18.40)	-72.20 (-72.80)	11/21/1751	0750 LT	3		Earthquake
Martinique and Barbados	14.40	-61.00	4/24/1767	0600 UT	3		Shocks

Table 1 (Continued)

Tsunami Origin	Latitude (N)	Longitude (E)	Date	Time	Validity rating	Earthquake magnitude and corresponding scale	Source type and brief description
Haiti	18.70 (18.60)	-72.63 (-72.80)	6/3/1770	1915 LT	4		Earthquake
Costa Rica	10.20	-82.90	2/22/1798		4		Earthquake
Venezuela	11.50	-66.90	3/26/1812		3		Earthquake
Jamaica	17.70 (18.00)	-76.30 (-76.50)	11/11/1812	1818 UT	3		Earthquake
Costa Rica, Nicaragua, and Panama	9.60 (9.50)	-82.20 (-83.00)	5/8/1822	0500 UT	4	Ms 7.6	Earthquake
Martinique	14.40	-61.00	11/30/1823	1130 LT	4		Earthquake
Martinique	14.20	-61.10	11/30/1824	0330 LT	3		Earthquake
Trinidad and St. Christopher	12.40 (12.40)	-61.60 (-61.50)	12/3/1831	1140 UT	4		Earthquake
Hispaniola and Cuba	19.97 (19.50)	-72.10 (-72.10)	5/7/1842	2200 UT	4	Ms 8.1	Earthquake (No effect in PR)
Guadelope	16.10	-62.20	2/8/1843	1435 UT	4	Mw 8.3	Earthquake induced landslide
Cumana, Venezuela	12.10	-63.60	7/15/1853	1415 LT	3	Ms 6.7	Earthquake
Honduras	16.00 (16.20)	-88.20 (-88.50)	8/9/1856		4	Ms 7.5	Earthquake

Table 1 (Continued)

Tsunami Origin	Latitude (N)	Longitude (E)	Date	Time	Validity rating	Earthquake magnitude and corresponding scale	Source type and brief description
St. Thomas, St. Croix, Puerto Rico, Dominica	18.10	-65.10	11/18/1867	1850 UT	4	Ms 7.5	Earthquake; along the north scarp of the Anegada Trough; 15 to 20 km SW of St. Thomas; St. Croix, St. Thomas, and Isla de Vieques formed a triangle around the epicenter; others believe it may have been of volcanic origin on Little Saba
Puerto Rico	18.10	-65.10	3/17/1868	1045 UT	4		Earthquake
Venezuela	10.80 (10.70)	-63.80 (-63.80)	8/13/1868	1137 LT	4		Earthquake
Lesser Antilles	15.50	-61.50	3/11/1874	0430 LT	4		Earthquake
Jamaica	19.60	-75.50	8/12/1881	0520 LT	4		Earthquake
Panama	10.00	-79.00	9/7/1882	1418 UT	4	Ms 8.0	Earthquake (Landslide?)
Haiti	19.70	-74.40	9/23/1887	1200 UT	4		Earthquake
Venezuela	11.00	-66.40	10/29/1900	0842 UT	4	Ms 8.4	Earthquake

Table 1 (Continued)

Tsunami Origin	Latitude (N)	Longitude (E)	Date	Time	Validity rating	Earthquake magnitude and corresponding scale	Source type and brief description
Jamaica	18.50 (18.20)	-76.60 (-76.70)	1/14/1907	2030 UT	4	Ms 6.5	Earthquake induced submarine landslide
Puerto Rico	18.50	-67.50	10/11/1918	1414 UT	4	Ms 8.25	Earthquake induced submarine landslide (subduction near the Brownson deep [Mona Canyon]; cables cut in several places)
Puerto Rico	18.50	-67.50	10/24/1918	2343 LT	4		After shock from the 10/11/1918 earthquake
Cumana, Venezuela	10.60	-65.60	1/17/1929	1152 UT	4	Ms 6.9	Earthquake (fault activity; slides and collapses)
Cuba	19.50	-75.50	2/3/1932	0616 UT	3	Ms 6.7	Earthquake
Hispanola	19.30	-68.90	8/4/1946	1751 UT	4	Ms 8.1	Earthquake
Puerto Rico	19.50	-69.50	8/8/1946	1328 UT	4	Ms 7.9	2nd shock from 8/4/46 earthquake; this one located 100 km to the NW
Barbados, Antigua, Dominica	15.80	-59.70	12/25/1969	2132 UT	4	Ms 7.7	Earthquake

Table 1 (Continued)

Tsunami Origin	Latitude (N)	Longitude (E)	Date	Time	Validity rating	Earthquake magnitude and corresponding scale	Source type and brief description
Leeward Is.	17.00	-62.40	3/16/1985	1454 UT	4	Ms 6.3	Earthquake (Possible Landslide)
Puerto Rico	19.23 (18.90)	-68.77 (-63.80)	11/1/1989	1025 UT	3	Ms 5.2	Earthquake
Costa Rica, Panama	9.90 (9.60)	-82.60 (-83.20)	4/22/1991	2156 UT	4	Ms 7.6	Earthquake
Venezuela	10.90 (10.60)	-63.50 (-63.50)	7/9/1997	1924 UT	3	Mw 7.0	Earthquake

Determination of IAS Tsunamigenic Potential

This study simulates events with the potential to have far-field (greater than 1000 km) destructive consequences and illustrates where impacts are possible. The proximity of the islands to each other makes it difficult for tsunami energy to propagate out of the region (or, in the case of origins outside of the region, to move into the Caribbean Sea). In order to determine if a tsunami is truly destructive at a location, high resolution bathymetry and a model with run-up capability are needed to predict the extent of inundation.

The tsunamigenic potential is an index that considers both the spatial frequency of tsunamigenic events and the geologic and tectonic regime of the region. This index helps understand where the next tsunamigenic event is likely to occur. In order to quantitatively measure the tsunamigenic potential of events it is necessary to place the data into bins. Through experimentation it was determined that 1-degree resolution is optimal because it is large enough to encompass more than one event but small enough to discern distinct regions of tsunami source areas.

The McCann [2004] tsunamigenic event source map (see Figure 1) is used to incorporate the geologic and tectonic regime of the region. Assigning a weighting system (Table 2) to the event source map, based on source type, allows it to be used as a relative tsunamigenic risk map. The weights, although subjective, allow for a quantification of the tsunamigenic event potential. High, medium, and low risk can be directly translated into weights (3, 2, 1 respectively) but slow earthquake potential, plate bending, or platform deformation regions as well as active faults, geologic belts and ridges also increase the potential for a region to produce a tsunami and are therefore assigned a weight of 1.5. This tends to be more important where areas of high, medium, and low risk overlap these regions.

Table 2 – Weight assignments to the tsunamigenic event source map [*McCann*, 2004].

High risk	**Medium risk**	**Low risk**	**Slow earthquake, belt or ridge, plate bending, platform deformation, active fault**
3	2	1	1.5

The weight attributes of each source type are applied to the 1-degree resolution grid (Figure 3) and when a grid cell or bin is not completely covered by a source type, the fractional area each source type encompasses is calculated. This is multiplied by the weight of the source type to determine the weight of the bin. Multiple weight types in a single bin are combined in superadditive process. For example, if a bin contains 1/3 high risk, 1/5 slow earthquake, and 1/3 platform deformation the resulting weight is: (1/3 * 3) + (1/5 * 1.5) + (1/3 * 1.5) = 1.6. The fractional areas can be both greater than or less than 1 since source types overlap. The final value of each bin is calculated by adding the spatial frequency to the potential bin weights (Figure 4).

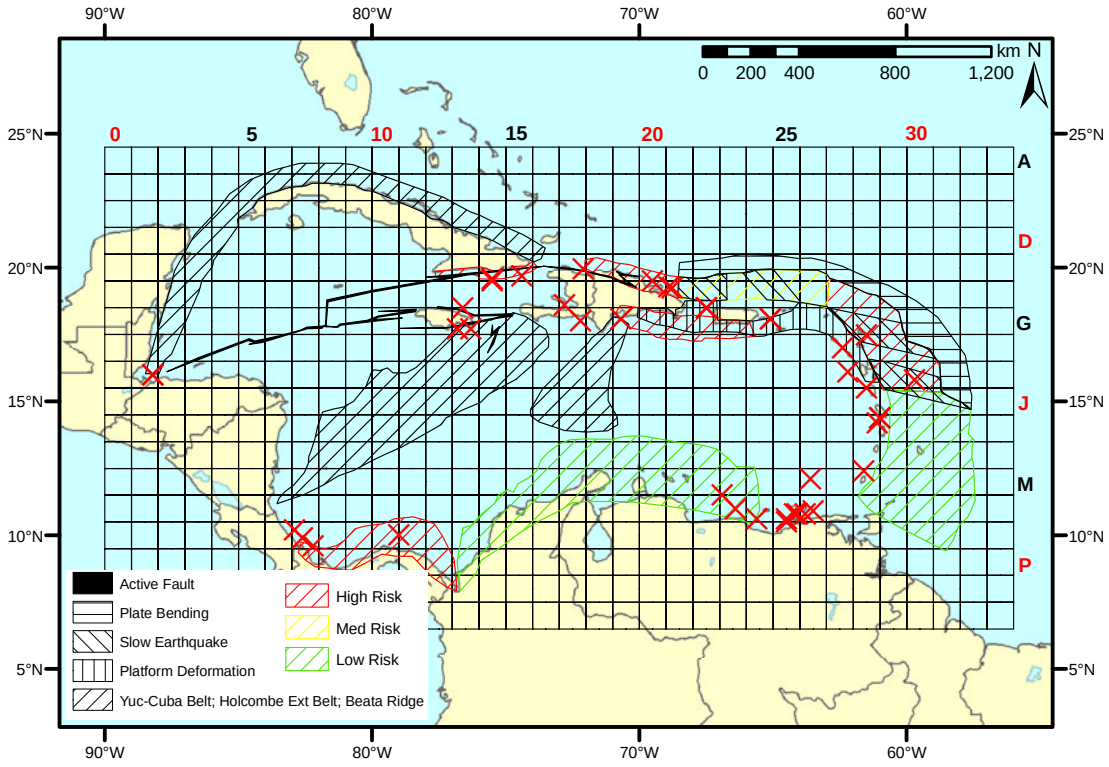

Figure 3 – 1-degree resolution grid, map of the IAS, historical tsunami origins, and tsunamigenic source regions. "X" represents the location of the historical origins. Historical origin data from O'Loughlin and Lander [2003] and NGDC [2005]. Tsunamigenic source data from McCann [2004].

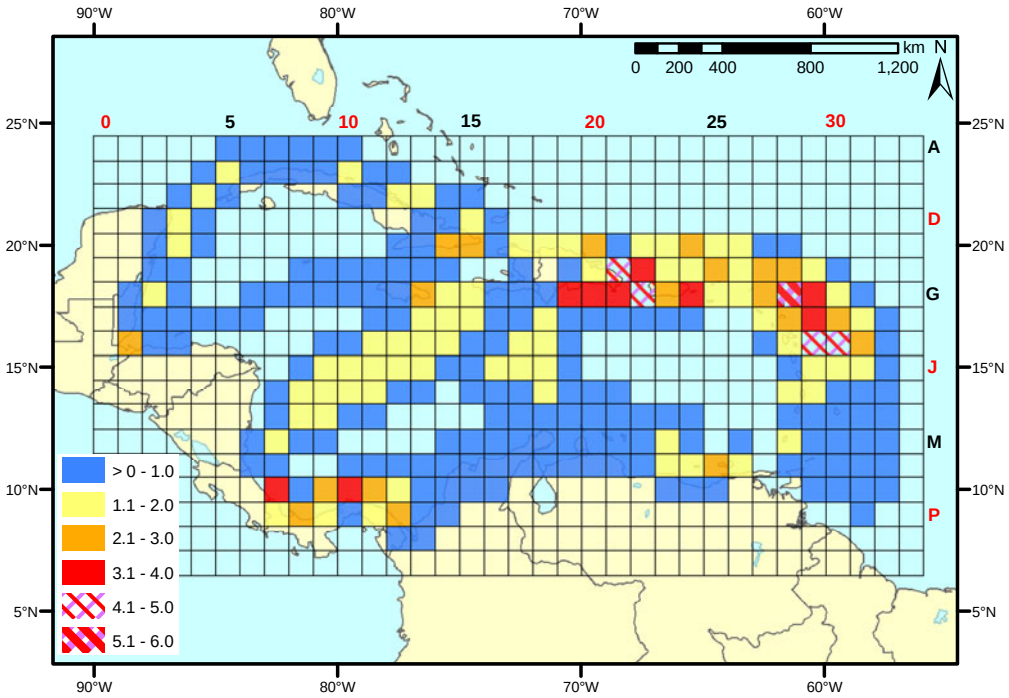

Figure 4 – Sector total weights. Result of binned historical tsunami origins and weight assignments to 1-degree resolution grid. Bins without coloring have a value of zero.

Modeling

The purpose of modeling historic tsunamis in this study is to understand tsunami propagation throughout the region, determine which coastlines are likely to be affected, and measure the travel time to those locations. The conditions used to initiate the simulations (Table 3) are the same for every historical tsunami simulation due to a lack of specific historical data. The tsunami origin coordinates were originally accurate to 0.1 degrees [*Dunbar*, 2005, personal correspondence], however 19 had to be adjusted as described in Methods ("Creation of tsunamigenic events list").

Two different models are considered for simulating the historical tsunamis. They are the US Navy Coastal Ocean Model (NCOM) and Tsunami Travel Time software developed by the Russian Tsunami Laboratory. The Tsunami Laboratory [*Gusiakov*, 2000] developed a tsunami travel time (TTT) program to calculate and plot isochrones in both the North Atlantic and IAS. The user-defined inputs are source type (point or ellipse), point of origin, and run time as well as different isochron display options. This program has the ability to calculate the travel time to 70 locations in the IAS but does not allow them to be user defined. The isochrones could be used to estimate travel time to other locations but they can be difficult to interpret. Therefore, this model/program has limited utility for this study.

The NCOM is a three dimensional model that can use a full-explicit, semi-implicit, or split-explicit time stepping integration scheme [*Martin*, 2000; *Morey, et al.*, 2003b; *Morey, et al.*, 2003a]. Others who have simulated historical tsunamis in the Caribbean use different models but these are based on the same basic equations used by the NCOM [*Mader*, 2001; *Mercado and McCann*, 1998]. Some of the basic equations of motion that NCOM solves are listed here in Cartesian coordinates from Morey et al. [2003b] (Equations 1 – 4). Although the Coriolis term is accounted for in the NCOM, its contribution is relatively small given the simulation duration (6 hr).

$$\frac{\partial u}{\partial t} = -\nabla * (\mathrm{V}u) + Qu + fv - \frac{1}{\rho_0}\frac{\partial p}{\partial x} + F_u + \frac{\partial}{\partial z}\left(K_M \frac{\partial u}{\partial z}\right) \tag{1}$$

$$\frac{\partial v}{\partial t} = -\nabla * (\mathrm{V}v) + Qv + fu - \frac{1}{\rho_0}\frac{\partial p}{\partial y} + F_v + \frac{\partial}{\partial z}\left(K_M \frac{\partial v}{\partial z}\right) \tag{2}$$

$$\frac{\partial p}{\partial z} = -\rho g \tag{3}$$

$$\nabla * \mathrm{v} = \frac{\partial u}{\partial x} + \frac{\partial v}{\partial y} + \frac{\partial w}{\partial z} = Q \tag{4}$$

$$\rho = \rho(T, S, z)$$

where,

u, v = velocity vector terms (m/s)	∇ = del operator	V = unit vector
Q = a volume source or sink term (m^3/s)	t = time (s)	f = coriolis parameter
ρ_0 = reference water density (kg/m^3)	p = pressure (Pa)	S = salinity
F_u, F_v = friction vector terms (N)	x, y, z = coordinate directions	
T = potential temperature (^oC)	g = gravitational acceleration (m/s^2)	
K_M = vertical eddy coefficient for momentum		

The 42 historical tsunamis are simulated with the NCOM using a leap-frog, semi-implicit time stepping integration scheme. This allows the use of larger time steps while maintaining stability and accuracy [*Morey, et al.*, 2003b; *Rueda and Schladow*, 2002]. However, if too large a time step is used and the Courant, Friedrichs, and Lewy (CFL) condition is violated, gravity waves (such as those modeled for this research) may be slowed down [*Bartello and Thomas*, 1996; *Dupont*, 2001]. The CFL condition is discussed later under the sub-section "Initial Conditions".

The NCOM is run in a barotropic mode with one depth averaged vertical grid cell. Tidal components are not included in any of the simulations and the temperature and salinity features are not utilized. All tsunamis are assumed to be shallow water waves. Sea boundaries are open and allow uninhibited passage. Land boundaries are closed and act as a vertical wall. Land is set to 20 m above sea level, and to avoid dry cell conditions as a wave reaches the coast, the minimum water depth is set to 4 m (see Appendix A – A note on dry cell issues and bathymetry alterations). Wave run-up on land is outside the scope of this study due to a lack of high resolution bathymetry and coastal topography for the study area, and a lack of high quality historical observations/measurements to ground truth model results. The grid resolution is set to match the bathymetry resolution (2 arc-min). It is not necessary to develop a higher resolution grid because the wave speed and hence travel time depends on the bathymetric resolution.

Bathymetry

ETOPO2 [*NGDC*, 2001] is a global, 2 arc-min resolution bathymetric and topographic dataset created by the NGDC. It is the highest resolution global bathymetry publicly available. Higher resolution is available for select areas of the Caribbean region. The Puerto Rico Tsunami Warning and Mitigation Program used the ETOPO2 and a National Ocean Service (NOS) multibeam dataset [*NGDC*, 2004] to create a higher resolution bathymetry data set [*Mercado-Irizarry*, 2005, personal correspondence]. The NOS dataset covers the U.S. Exclusive Economic Zone (EEZ) around Puerto Rico at 15-second resolution. However, to avoid artificially inducing a difference in model results based on a difference in bathymetric resolution, only ETOPO2 bathymetry is used in this study.

Initial conditions

Known as an inverse tsunami problem, a method of determining some initial conditions for a tsunamigenic event is to back calculate them from historical observations

of tsunami impacts [*Mader*, 2001; *Murty*, 1977]. However, the historical record for tsunamis in the Caribbean region is poor and it is difficult to reconstruct such events with any accuracy. Some works have used a seismic or initial condition model [*Mercado and McCann*, 1998; *Meyer and Caicedo O.*, 1998] to determine the initial wave parameters while other models such as NCOM and MOST (Method of Splitting Tsunamis) can also run with user-defined initial conditions. For this study, several sensitivity tests are run to determine initial wave amplitude and e-folding radius, bottom roughness coefficient, model time step, surface field output interval, and total run time. Appendix B describes the sensitivity tests in detail and the results are summarized in Table 3.

The surface field output interval depends on the temporal resolution required to consistently identify the exact moment of tsunami impact. A surface field output interval of 45 sec is sufficient to obtain adequate resolution. The sensitivity experiments converged on a model time-step of 7.5 sec and a grid spacing of 2 arc-min, which also satisfies the CFL condition. The CFL condition states that the time step must be smaller than the time it takes for a wave to propagate from one grid point to the next (Equation 5). Based on a celerity of 800 kph, two time steps will pass as a wave moves from one grid point to another.

$$C < 1$$
$$C = \frac{c\Delta t}{\Delta x} \qquad (5)$$

where,
c = wave celerity (m/s) delta t = time step (s) delta x = grid space (m)

Table 3 – Sensitivity test results summary

Initial amplitude (m)	e-folding radius (m)	Bottom roughness coefficient	Time step (s)	Surface field output interval (s)	Total run time (hr)
4	10,000	0.003	7.5	45	6

The shape of the initial wave adds the most uncertainty to the results of the simulations presented here. However, too little is known about the initial conditions of all of the events simulated. Therefore, in order to compare the output from each model run, the same initial conditions are used to initialize all of the historical tsunamis simulations. Zahibo et al. [2003b] has also used the same initial conditions for 19 historical events, and a time step and grid spacing of 6 sec and 3 km, respectively.

Each tsunami is modeled as a point source using a normalized Gaussian dome with an amplitude of 4 m and an e-folding radius of 10 km (Table 3; Equations 6 – 11). This assumes that the entire water column is composed of an incompressible fluid and that this generation process is instantaneous [*Okada*, 1985]. This assumption is based on previous works such as Kowalik and Whitmore [1991], Shuto [1991], and Mercado and McCann [1998].

The initial wave is produced by the formula,

$$wave(i,j) = amp * e^{\left(\frac{-r^2}{2*R^2}\right)} \quad (6)$$

where amp is the initial height of the sea surface above mean sea level in meters; R is the e-folding radius in meters; and i and j are grid coordinates.

$$r = x^2 + y^2 \quad (7)$$

$$\begin{aligned} x &= (i - i_0) * dx(i,j) \\ y &= (j - j_0) * dy(i,j) \end{aligned} \quad (8)$$

$$dx(i,j) = 111.1950 * \cos d(alat(i,j)) * \frac{1000}{30} \quad (9)$$

$$dy(i,j) = 111.1950 * \frac{1000}{30} \quad (10)$$

$$alat(i,j) = 7 + \frac{j-1}{30} \quad (11)$$

Determination of Coastal Grid Points (CGP), Population Data Incorporation, and Time Series Analysis

Once the simulations are performed, custom programs, written in Research Systems, Inc Interactive Data Language (RSI IDL), are used to determine impact and calculate the travel time to the coastlines throughout the IAS. One program uses the ETOPO2 bathymetry data to identify the first grid point just off shore. This produces 10,623 grid points in an area approximately from 7ºN, 59ºW to 36ºN, 98º W (Figure 5A). A close up of CGP's around Puerto Rico illustrates their resolution (Figure 5B). The other custom program performs an automated time series analysis and is discussed later.

Figure 5A – All 10,623 coastal grid points used in the initial time series analysis study.

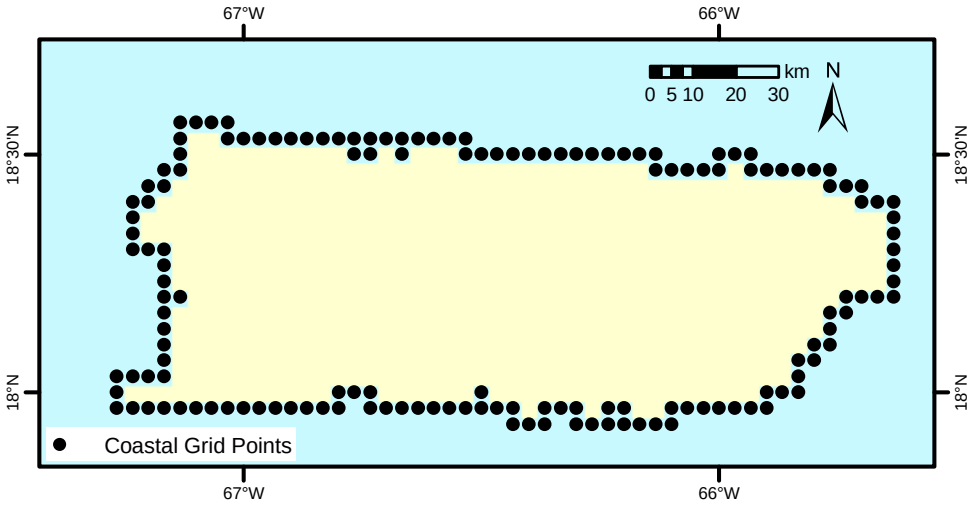

Figure 5B – Inset of figure 5A; Close-up view of CGPs around Puerto Rico

Population data is obtained from the Latin American and Caribbean Population Database [*CIAT, et al.*, 2005]. This database encompasses the Caribbean and South and Central American regions at a mean resolution of 33 km. The resolution varies from country to country and is generally 9 – 53 km. This data is incorporated into each coastal grid point using an euclidian allocation technique (with ESRI ArcGIS ©), where each CGP is assigned the value of the population cell closest to it. The CGP's bordering the

continental United States are not used because it is shown later in the results that the travel time to where the continental US is impacted by the simulated tsunamis is at least 4 hr (Figure 6). Sea level gauges throughout the Caribbean are capable of warning this coastline.

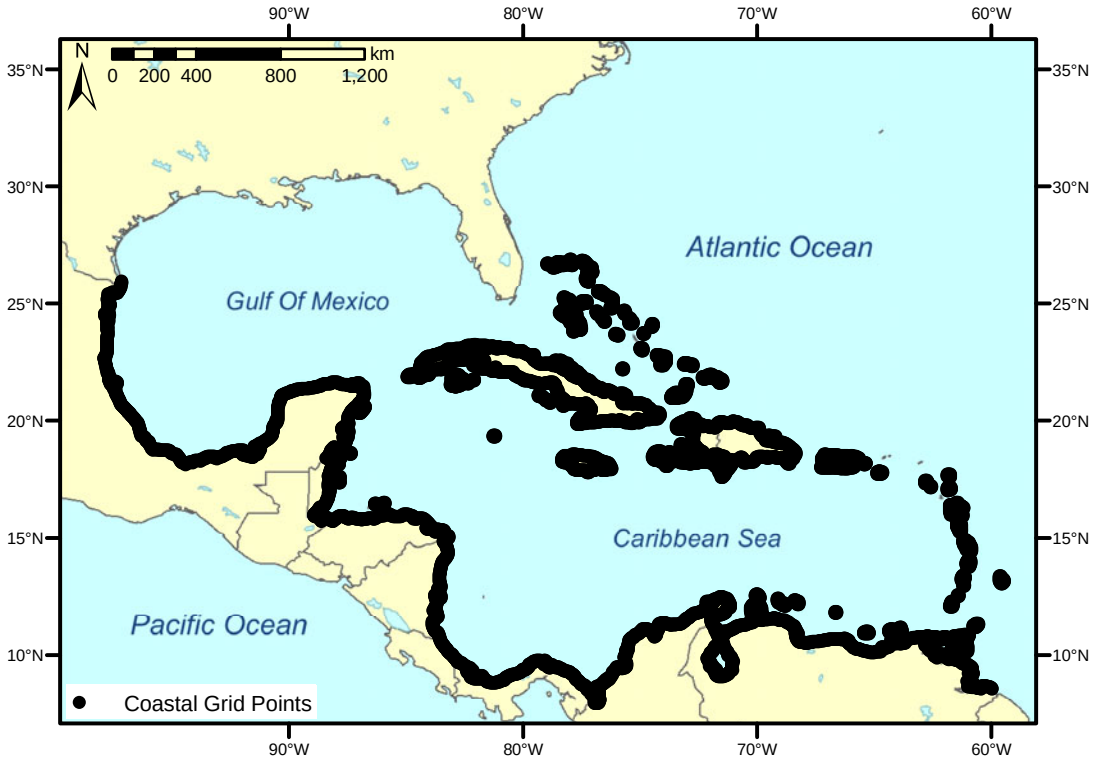

Figure 6 – 8,009 CGP's with attributed population data. The CGP's boardering the continental United States seen in 5A are not shown here.

Efficient use of a limited number of sea level gauges requires that each gauge warn the greatest number of people possible. To accomplish this, population centers are identified using the population data just described. A population center, due to the high and variable resolution of the population data set, is defined as a CGP having a population of over 500. Once these points are identified, the dataset is edited to eliminate replicates and points in close proximity to each other. Using this method, it is necessary to supplement this list with major tourist locations since these do not necessarily have high populations. These locations are also referred to as population centers. The resulting dataset is summarized in table 4 and displayed in figure 7.

Table 4 – List of population centers. * denotes added tourist location; Coordinates from www.fallingrain.com and adjusted to nearest CGP.

St. Johns, Antigua and Barbuda*	Near Old Harbour, Jamaica
Basseterre, Saint Kitts and Nevis*	Kingston, Jamaica
Basse-Terre, Guadeloupe (France)*	Ponce, Puerto Rico
Christiansted, St. Croix (Virgin Islands)*	Les Cayes, Haiti
Marigot, Sint Maarten (Neth. Ant.)*	Mayaguez, Puerto Rico

Table 4 (Continued)

Roseau, Dominica*	Fajardo, Puerto Rico
Fort-de-France, Martinique (France)*	Santo Domingo, Dominican Republic
Castries, St. Lucia*	Near Jeremie, Haiti
Bridgetown, Barbados*	Near St. Marc, Haiti
Kingstown, St. Vincent and the Grenadines*	Cap-Haitien, Haiti
St. George's, Grenada*	Santiago De Cuba, Cuba
Puerto Limon, Costa Rica*	South Beach,Bahamas (New Providence)
Portobelo, Panama*	Near Barcelona, Venezuela
Cancun, Mexico*	Near PuertoCabello, Venezuela
Playa del Carmen, Mexico*	Near Carupano, Venezuela
Willemstad, Curacao*	Pampatar, Venezuela
Cartagena, Colombia	La Ceiba, Honduras
Barranquilla, Colombia	San Juan, Puerto Rico
Santa Marta, Colombia	Port-of-Spain, Trinidad and Tobago
near Oranjestad, Aruba	Havana, Cuba
Puerto Cortes, Honduras	Manzanillo, Cuba

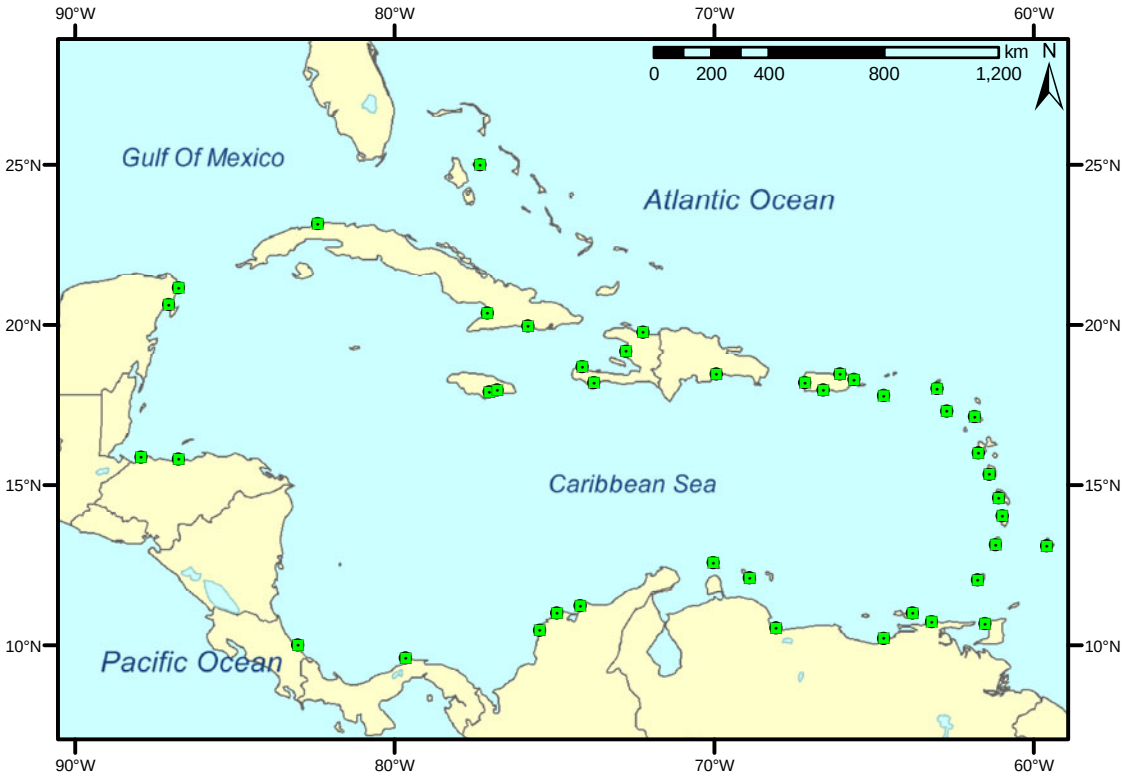

Figure 7 – Population centers (represented by the squares).

The travel time and associated data corresponding to each grid point are extracted from the model output and written to files in a two step process also using a RSI IDL program. Step one reads in data for all grid points, one record at a time. After this is

completed, the second step writes a sea surface elevation time series file for every point and one event file containing the travel time and associated data for each GCP. This threshold is used to determine if the CGP is impacted by the simulated tsunami. The CGP is considered to be impacted only if the threshold is met. Travel time is defined as when the first peak or trough, above a threshold (Equation 12), reaches the CGP.

$$\left(H_n - H_{n-2}\right)^2 > 0.00001 \tag{12}$$

Both peaks and troughs are considered to determine travel time because, due to the initial condition uncertainty, phase error may be present. A peak or trough is identified when the time series meets the criteria set forth in both equations 12 and 13. These equations, in conjunction with the program just described, can accurately identify impacted locations and the first peak or trough in a surface elevation time series (Appendix C).

$$\frac{H_{n+1} - H_n}{H_n - H_{n-1}} < 0 \tag{13}$$

where, H = sea surface height and n = record number

Sea Level Gauge Location Determination

A sea level gauge for a tsunami warning system should be positioned to maximize warning time. Several factors are considered to calculate warning time. These include population centers, locations where a tsunami may occur, travel time or propagation speed, and wave dissipation. The Pacific Tsunami Warning System is designed to detect a tsunami within 30 min after the generating earthquake [*Bernard, et al.*, 2001]. The IAS TWS proposal, accepted by the IOC (Intergovernmental Oceanographic Commission), recommends at least 15 min of warning time [*IOC-UNESCO*, 2005]. This study calculates the warning time by subtracting the travel time to the population center from the travel time to a sea level gauge. A population center is considered to be warned if it can be notified within 30 min after tsunami generation. In general, the closer the gauge is to the tsunami origin, the more warning time available to population centers.

Knowing where a tsunami will originate is essential to determining where a gauge should be installed. In Methods ("Determination of IAS Tsunamigenic Potential"), the relative risk of where tsunamigenic events will occur is shown (see Figure 4). The McCann [2004] tsunamigenic source map, used in part to create the tsunamigenic risk map, appears to have a gap in tsunami risk just north of Venezuela in sectors N25 and N26 (see Figure 3). This is assumed to be a gap because, based on his methodology for classifying risk or source areas and the frequency of historical tsunamis occurring in those sectors, they should be covered by a region of low risk. This additional low risk value is added to the value of sectors N25 and N26 as if completely covered by a low risk area. The bins or sectors without a value are discarded and the values of the remaining sectors, ranging from 1.00E-4 – 5.05, are relatively evenly distributed. The upper ~ 5%, or 15 of these sectors, are considered to be where tsunami-genesis risk is relatively highest (Figure 8).

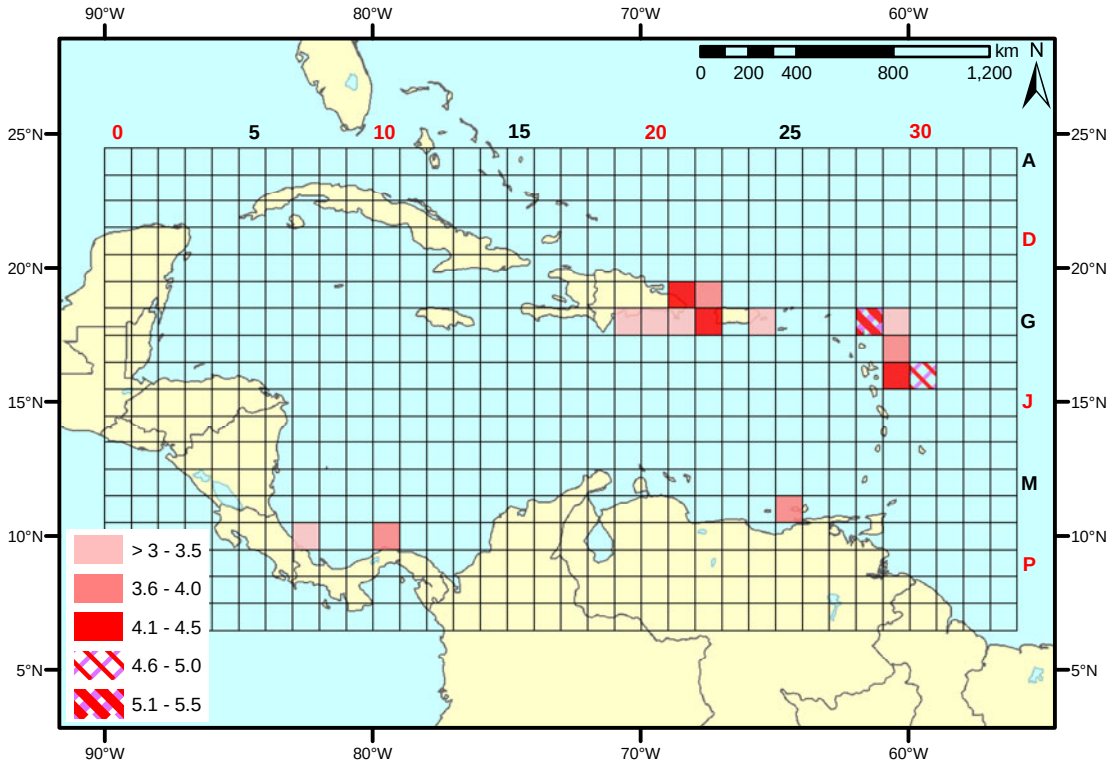

Figure 8 – Top 5% of risk sectors. Note that the color bar shown here is different than that shown in figure 4.

The NCOM is not used to model events from the center of the risk sectors because a tsunami many not necessarily originate there. The NCOM is specific in this regard where as an isochron system is general and renders conservative estimates. Isochron development and validation using the NCOM are discussed in Appendix D. Travel time is measured from the center of the shaded sectors in Figure 8 to the nearest point of land and to the population centers using a series of isochrones. The recommended gauge location corresponds to the point of land nearest to the center of the relatively higher risk tsunamigenic sectors. With this strategy, each point closest to a high-risk sector should receive a sea level gauge resulting in 15 locations. However, some sectors are closest to the same point of land and the final number of locations identified is discussed later. For simplicity, gauge locations are referred to as the sector they correspond to.

Location Priority for Coastal Sea Level Gauges

Through an iterative experimental process a simple decision matrix is developed to evaluate the relatively highest risk sectors in the following categories:

i. Sector risk value
ii. Number of population centers the sector gauge can warn in time
iii. Number of population centers less than 1000 km away
iv. Number of sectors closest to one potential gauge location
v. Number of sectors sharing a border

Each sector is assigned a rank in all categories, the ranks are added together, and the sector with the lowest number is assigned an overall rank of 1, the second lowest a rank of 2, etc. The final priority list includes all aspects with equal consideration since all ranks are simply added together.

The sector risk values are ranked so the sector with the highest relative risk receives first priority. This means that, to a first order, a sea level gauge is most useful within or nearest to a sector that is the most likely to generate a tsunami. This location, though, may not be able to warn as many population centers as another, reducing its effectiveness.

According to the warning time criteria of 30 min, each location has the potential to warn a certain number of population centers. Some locations can warn all but 1 while others do not have time to warn up to 8 centers. However, in the Caribbean, the risk to population centers is low if they are at least 1000 km away from the tsunami origin [*Zahibo, et al.*, 2003b]. A direct line distance is used in this study, since the resulting complex island reflections and refractions soon after tsunami generation make it difficult to perform accurate ray tracing. The list of population centers each gauge can warn is reduced to those less than or equal to approximately 1000 km away from the center of the sector. The sector and corresponding gauge that warns the most population centers less than or equal to approximately 1000 km away is given higher priority.

In some cases, different risk sectors are closest to the same point of land (Figure 10). It is more efficient to install a sea level gauge on a point of land closest to more than one sector. This gives the gauge the ability to warn of a tsunami originating from multiple sectors. Higher priority is allocated to sectors that share a gauge location.

Population centers near multiple higher risk sectors have increased potential to be impacted by a tsunami. To account for this sector density or clusters of higher risk sectors, the number of borders each sector shares with another sector is counted. In this manner, higher priority is skewed towards the clusters of risk centers.

RESULTS and DISCUSSION

This project is built on a series of sub-studies whose results have been used to develop methodology. The results of this systematic approach to assess sea level gauge location and priority should assist in developing a tsunami warning system for the Intra-Americas Sea. Here we review the modeling decisions and results, vulnerability of the IAS coastline to tsunami impact, sea level gauge installation location priority, and currently operational sea level gauges within the IAS.

Modeling Validity

Major aspects of modeling include choosing the correct model, the accuracy of the initial conditions, and the validity of assumptions. Depending on the model used for both propagation and initial displacement there may be differences in calculated wave amplitudes. However, previous studies have not evaluated whether the choice of model affects travel time estimates [*Mercado and McCann*, 1998; *Whitmore*, 2003; *Zahibo, et al.*, 2003a]. Travel times estimated here, in general agree with those calculated in both Weissert [1990] and Mercado and McCann [1998] and observed by Reid and Taber [1919].

Weissert [1990] developed an isochron time chart for the 1867 Virgin Islands tsunami (see Table 1). Travel times are in reasonable agreement for open areas, but less in regions of more complicated bathymetry. For example, he estimates a travel time of 100 – 120 min to the Northeast coast of Cuba, but the NCOM travel time calculation was approximately 250 – 350 min. Here, there is a significant difference between the travel times to the coast and between the ranges of travel times. This may have been a result of a coarser bathymetry used in Weisserts' study (ETOPO5) or the breakdown of that model's ability to simulate a tsunami in shallow water, as explained by the author.

Mercado and McCann [1998] simulated the 1918 Puerto Rico tsunami (see Table 1) and show a sea level time series for three Puerto Rico locations: Aguadilla, Mayagüez, and Boqueron. These three time series are compared to those generated from the NCOM output. As in this study, travel time to these locations is taken as the time corresponding to the first peak or trough on the Mercado and McCann [1998] sea surface elevation time series. Reid and Taber (1919) report observations of the 1918 Puerto Rico tsunami. The travel times they and Mercado and McCann [1998] report generally agree with those produced in this study (Appendix E).

Any discrepancies with Mercado and McCann [1998] may be because they use a higher bathymetric and grid resolution, more accurate bathymetry, and run-up capability (Mercado and McCann use a 3 arc-sec grid resolution where a 2 arc-min resolution is used in this study). In addition, the location and shape of the initial wave is also different. They generate the tsunami along a multi-segment fault line whereas it is considered a point source here.

Tsunami Travel Time and IAS Coastline Vulnerability

Based on the temporal frequency of historical tsunamigenic events, this region is due for another destructive tsunami [*O'Loughlin and Lander*, 2003; *Pararas-Carayannis*, 2004; *Zahibo, et al.*, 2003b; *Zahibo, et al.*, 2003a]. This work attempts to point out where the next tsunami is likely to occur and where a sea level gauge should be located to give the largest number of people the greatest warning time.

Several works have discussed the local nature of devastating effects from many historical tsunamis [*Mercado and McCann*, 1998; *Meyer and Caicedo O.*, 1998; *Pararas-Carayannis*, 2004; *Zahibo, et al.*, 2003a]. It has also been shown that tsunamis generated in the Caribbean can be destructive as far away as 2 – 3 hr [*Zahibo, et al.*, 2003b]. In order to determine the IAS coastline vulnerability, here it is assumed that these tsunamis can be destructive up to 6 hr away.

Figure 9 displays where 42 historical tsunamis have impacted and indicates the frequency of impact at those locations. To show where the continental United States has had the potential to be impacted, all 10,623 CGP's are included in figures 9 – 11. Some areas are never hit and some are hit by every tsunami modeled. The two main factors controlling this are the origin location and bathymetry. To incorporate travel time with impact frequency and travel time, the mean travel time is displayed in figure 10. It can be inferred that where the mean travel time is low (≤ 30 min), the majority of tsunamis impacting that location originated close to it. The opposite can be inferred where the mean travel time is high (> 1.5 hr).

The median travel time helps understand what locations may be more vulnerable to a regional tsunami regardless of impact frequency (Figure 11). Compared to mean travel time, the median tends to be lower at locations that are hit more frequently. The mean travel time is longer than the median 64% of the time, which means that there are more locations that are hit more often from tsunamis that travel long distances. This is an indication of their vulnerability to regional tsunami impact.

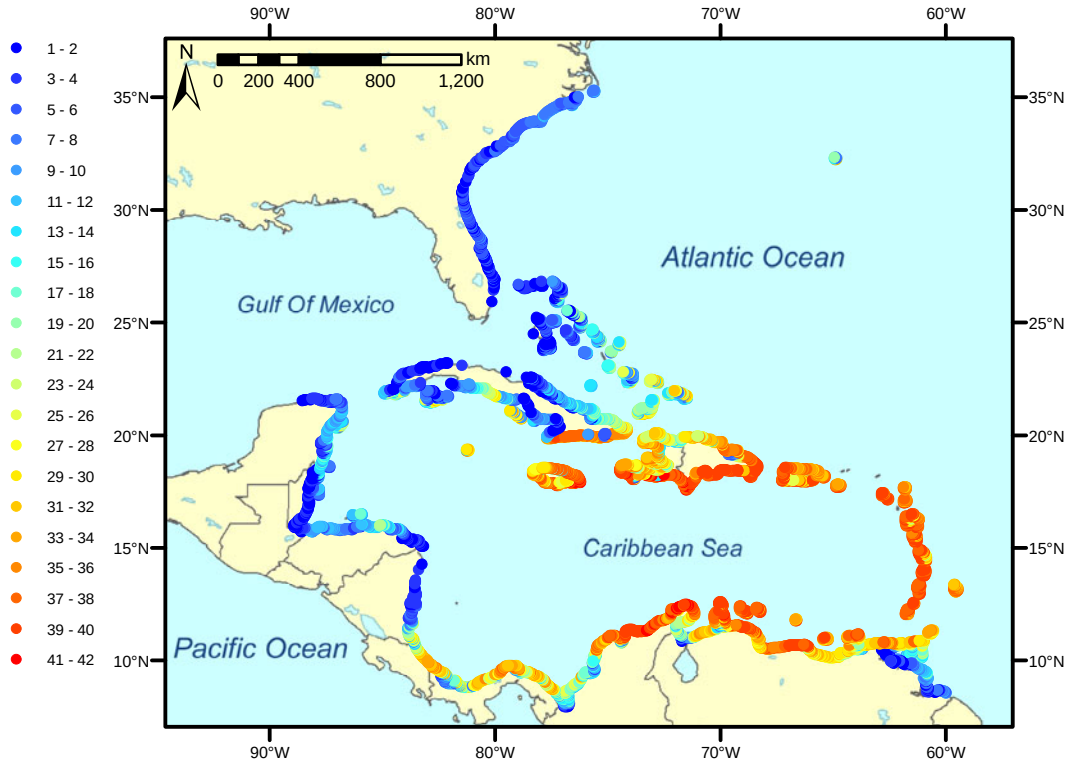

Figure 9 – Impact frequency. Locations where a CGP was impacted by at least one of the 42 historical tsunamis. Colors denote frequency of impact at that location.

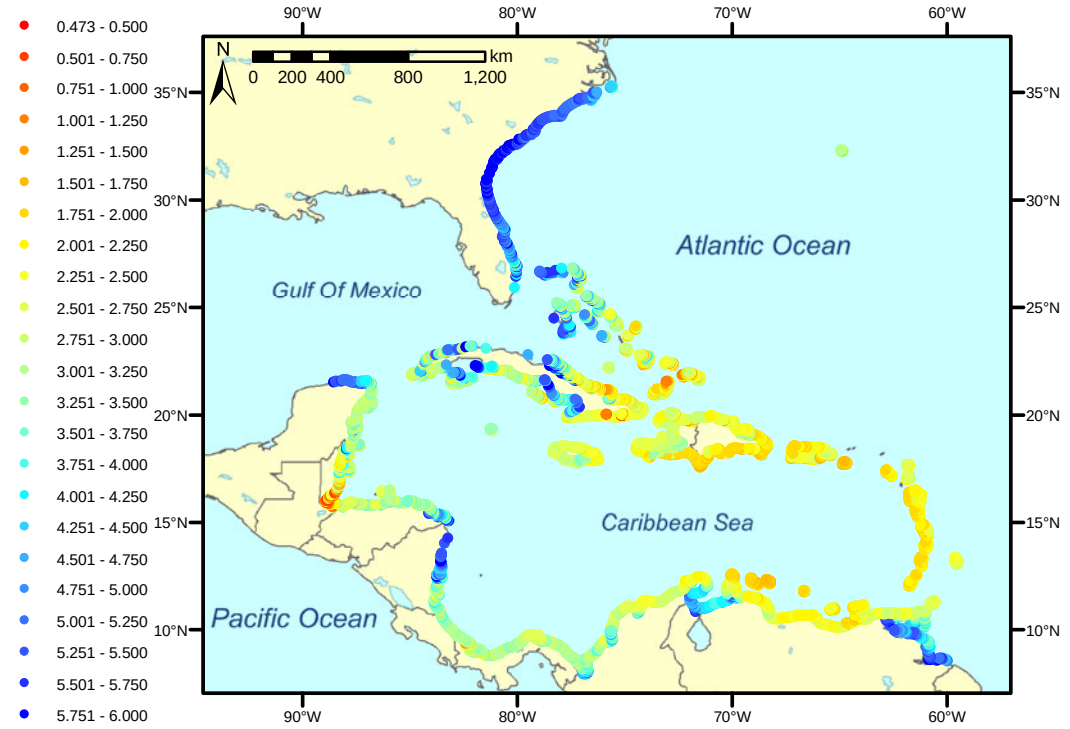

Figure 10 – Mean travel time. Similar to figure 9 but here colors denote mean travel time in hours to that location.

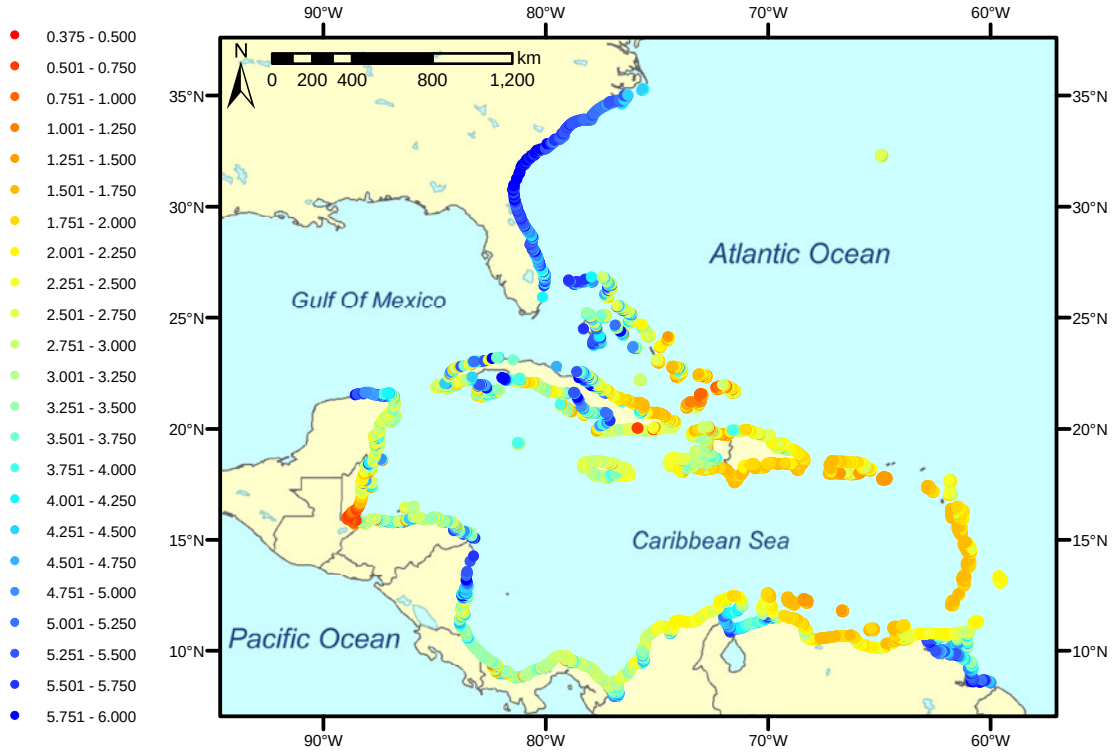

Figure 11 – Median travel time. Similar to figure 9 but here colors denote median travel time in hours to that location.

Sea Level Gauge Location Priority

This study uses a two-pronged approach to determine the IAS regional tsunami risk. One assumes that a tsunami impact has the potential to be destructive up to 6 hr from the origin and the other assumes that a tsunami will only be destructive within approximately 1000 km from the origin. The former is important when determining what locations have historically had the potential for impact and the latter is considered when optimizing and prioritizing gauge locations.

Table 5 summarizes the rank of the higher risk sectors by the factors dictating the installation location priority. These ranks were combined in a linear fashion to determine an overall rank (Table 6). In the event two sectors have the same value, they are assigned the same rank. The gauge corresponding to the sector with the highest overall rank should be installed first. The insertion the low risk area over sectors N25 and N26 described in Methods ("Sea Level Gauge Location Determination") led to the addition of sector N25 to the list of relatively higher risk sectors.

Table 6 shows the prioritized list of initial locations for sea level gauges recommended to provide an efficient warning system. When two sectors share the same potential gauge location and have a different priority, the higher priority rank is applied to both sectors. Several sectors share priority and two different locations are recommended for sector G22. Priority sharing can be resolved in a number of ways. The importance of one factor can be increased or decreased, a multiplier can be applied to a factor, or other factors can be included in the decision matrix such as site infrastructure, security of a site, and maintainability. As explained earlier, this study assesses regional

tsunami risk of impact based on historical tsunamigenic events, the geologic and tectonic regime of the region, wave propagation dynamics, and the location of major population centers within a range of 1,000 km from the center of the higher risk sectors. Nonetheless, a complete warning system should also consider exactly where run-up and inundation would occur and to what extent.

Table 5 – Decision rank matrix. The sectors are arranged in alphabetical order.

Sector	Risk value	# of sectors with same closest land	# of sectors sharing a border with sector of interest	# warned < 1000 km away	Total
F21	5	3	1	2	11
F22	8	3	1	5	17
G19	15	3	2	4	24
G20	13	3	1	1	18
G21	11	3	1	3	18
G22	3	3	2	4	12
G24	14	3	3	6	26
G28	1	2	2	8	13
G29	12	2	1	9	24
H29	9	1	1	10	21
I29	4	1	1	8	14
I30	2	1	2	11	16
N25	6	3	3	7	19
O7	10	3	3	12	28
O10	7	3	3	12	25

Table 6 – List of initial sea level gauge locations recommended for a tsunami warning system. Locations are listed in order of highest to lowest priority groups. Location coordinates should only be used as a guideline.

Sector	Approximate location for gauge installation	Priority
F21	Arena Gorda, Dominican Republic (-68.52, 18.78)	1
G22	Isla Mona, Puerto Rico (-67.89, 18.09) or Boqueron, Puerto Rico (-67.17,18.02)	2
G28, G29	Barbuda (-61.80,17.64)	3
H29, I29, I30	La Desirade, Guadeloupe (-61.05, 16.32)	4
F22	Aquadilla, Puerto Rico (-67.15, 18.50)	5
G20 G21	Boca Chica, Dominican Republic (-69.61, 18.45) Isla Saona, Dominican Republic (-68.57, 18.11)	6
N25	Punta Arenas, Venezuela (10.9667, -64.4)	7
G19	Las Calderas, Dominican Republic (-70.5, 18.20)	8
O10	Portobelo, Panama (-79.65, 9.55)	9
G24	Isla de Vieques, Puerto Rico (-65.45, 18.10)	10
O7	Punta Manzanillo, Costa Rica (-82.64, 9.63)	11

Changing the number and location of population centers, as well as the decision criteria, may affect the suggested gauge priority. The population centers were selected based on population and tourism alone and may not need to be warned if they are protected by a wide continental shelf or other wave energy dissipation medium. In addition, the number of warnable population centers will increase if tsunamis have destructive capability at distances greater than 1000 km. Answers to these possibilities require higher resolution bathymetry, modeling more origins (including those that are hypothetical in areas of higher tsunamigenic potential), as well as calculating run-up and inundation.

The installation location coordinates are dependant on where the center of the higher risk sectors are and should therefore only be used as a guideline. The number of initial gauges recommended for installation may change if the definition of a high risk sector changes. The locations selected are based on the top 5% of the relatively higher risk sectors and do not constitute a finite list. Additional areas should be considered for sea level gauge installations, specifically Venezuela near Margarita Island, the southeast coast of Jamaica, and the southeast coast of Cuba.

Although table 6 lists only one location per sector, in some cases 2 or 3 sensors may be more effective. It may take only one gauge to determine if the seismic event caused a tsunami, but this is a binary approach. It may not give enough information as to where else and to what extent the tsunami may impact on a larger scale. More sea level gauges can be used to detect a tsunami originating on either side of an island, and/or also improve travel time and wave height predictions.

A more general approach to a warning system is the installation of DART buoys. They have the potential to yield better predictions because, unlike a coastal sea level gauge, they receive a tsunami signal without being compromised by local effects or coastal noise. Although a DART buoy may prove more useful in propagation and wave height prediction as well as cover a larger origin area, they may not provide as much warning time. This approach cannot warn locations that are the same distance from the tsunami origin as the buoy, because a tsunami will reach both locations at about the same time. This reduces their usefulness and requires that a robust warning system employ a combination of both coastal and open ocean sea level gauges.

Operational Sea Level Gauges in the Caribbean

Figures 12a and b show the locations of the fully operational and proposed gauges as well as the recommended locations in table 6. Approximately 60 sea level gauges have been installed in the Caribbean and adjacent regions over the last 10 years and were thought to be operational. Of these, only 17 are currently operational and transmitting data, 16 are not operational but the equipment is accounted for, 10 are questionably operational, and the remaining are either no longer operational or gone [*Air-Sea Monitoring Systems*, 2006; *Henson and Wilson*, 2005]. The IAS TWS proposal [*IOC-UNESCO*, 2005] recommends that 31 sea level stations become tsunami ready to operate within the IAS TWS.

The PRSN begun installing 10 sea level gauges [*von Hillebrandt-Andrade*, 2006, personal correspondence] and the NOAA National Ocean Service (NOS) has 7 sea level gauges installed throughout Puerto Rico and the US Virgin Islands. Two of the PRSN

tsunami ready gauges (Aguadilla and Isla Mona) and one of the NOAA NOS gauges (9752695) coincide with locations recommended by this study.

Any sea level gauges used for tsunami warning must be supported as a part of an operational system and regularly maintained. Support can come from a variety of sources because coastal sea level gauges are typically a component of a larger station capable of collecting various other data including wind speed and direction, barometric pressure, precipitation, salinity, dissolved oxygen, water clarity, solar radiation, and current flow. These stations therefore have many applications, such as storm surge warnings and studies, hurricane forecasting, geostrophic current analysis, land subsidence, plate tectonics, commercial and recreational fishing and diving, search and rescue operations, and commercial shipping.

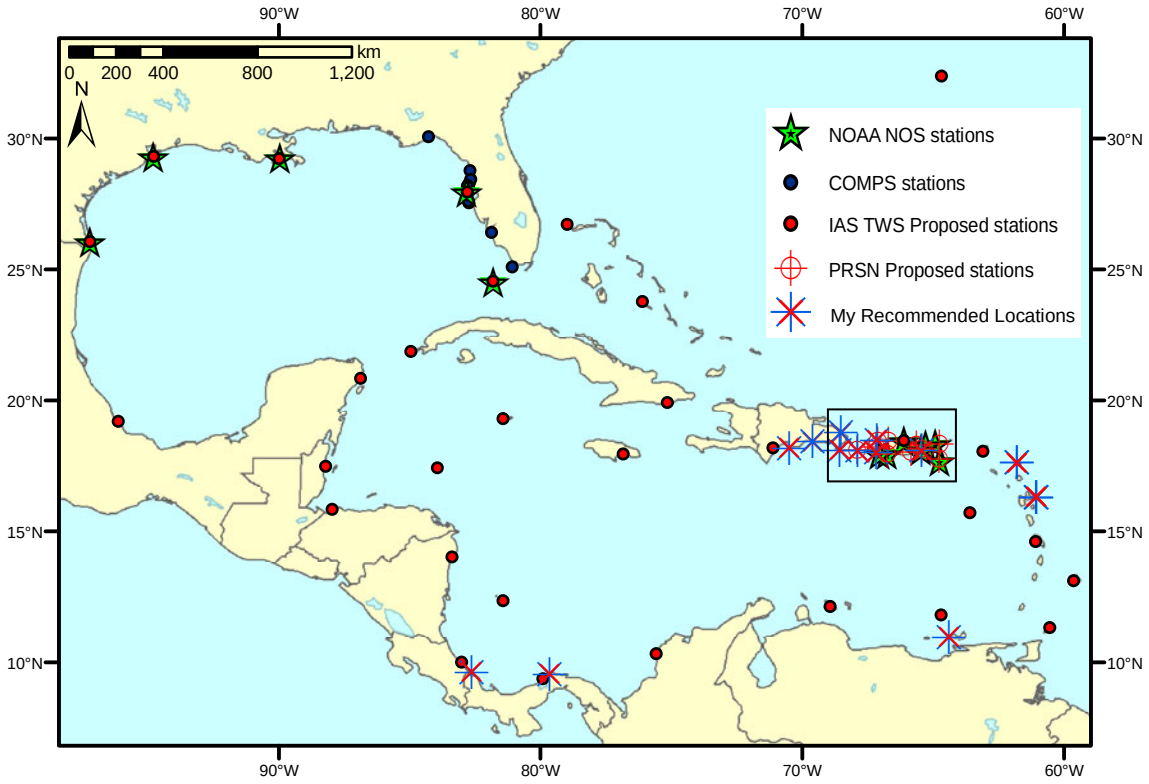

Figure 12a – Operational and recommended sea level gauge stations in the IAS. There are 12 operational sea level gauges sponsored by the NOAA NOS, 11 recommended locations for sea level gauges, 31 IAS TWS proposal locations, 10 PRSN locations proposed for the Puerto Rico Tsunami Ready Tide Gauge Network, as well as 11 Coastal Ocean Monitoring and Prediction System (COMPS) gauges shown in the figure. The alternate location for sector G22 is also shown. Box in northern Caribbean is enlarged in figure 12b.

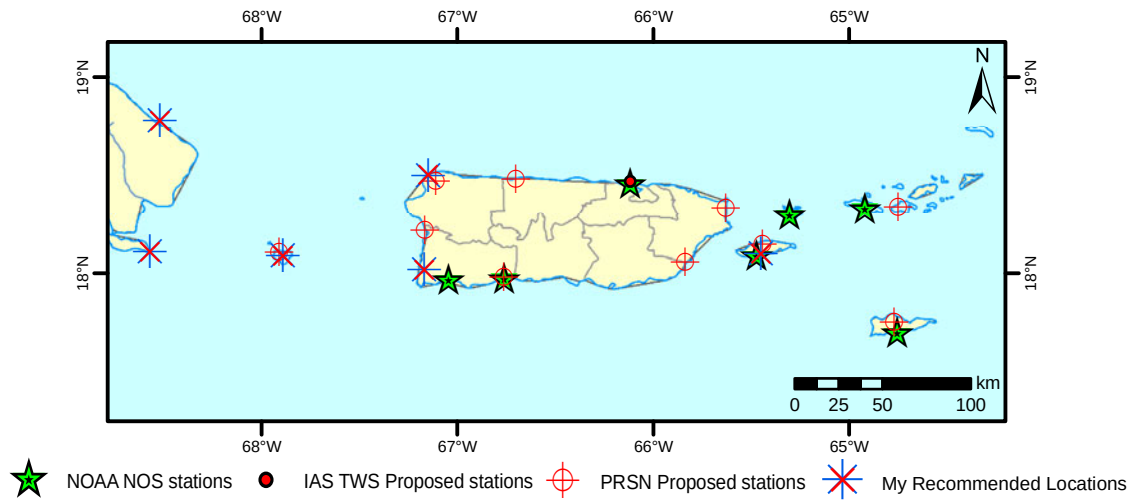

Figure 12b – Inset of figure 12a; Close up view of stations around PR, the USVI, and the Dominican Republic. Illustrates the proximity of the locations recommended in this study with those already installed by NOS and those recommended by the PRSN. Note where the locations recommended in this study overlap the NOAA NOS and PRSN proposed locations.

CONCLUSIONS and RECOMMENDATIONS

The goal of a tsunami warning system is to mitigate loss of life and property caused by a tsunami. Different types of systems/networks are currently being successfully employed to measure, record, and telemeter both oceanographic and meteorological data for tsunami warning. This study determined prioritized locations for coastal sea level gauges in the IAS based on tsunami generation risk factors, tsunami propagation throughout the region, population distribution, and tsunami travel time to population centers. These locations will give the maximum warning time to the largest number of people in the most efficient manner.

A database of all sea level gauges installed or thought to be installed was compiled and used to coordinate the recommended locations. The expansion of the IAS regional tsunamigenic event risk analysis was accomplished by combining the spatial frequency of 42 historical tsunamis with a modified tsunami source map from McCann [2004]. This study assumes that the 42 tsunamis were generated by either a dip/slip earthquake or massive slide/slump and were regionally destructive. Each historical tsunami was modeled with the NCOM enabling estimations of where historical tsunamis have had the potential to affect and the travel time to 10,623 coastal locations. An animation of each simulation is available from the author upon request. Throughout this work a GIS database was created which will also be useful to those planning the IAS tsunami warning system.

This study established that, initially, 12 sea level gauges are recommended, and 3 of these locations already have or are planned to have a gauge. These locations correspond to the land closest to the center of the relatively higher risk sectors and should serve as a guide for installation location. The list provided in Table 6 is not all-encompassing, but represents a start and will primarily warn against tsunamis that originate in the higher risk sectors. To determine exactly where a sea level gauge should be installed a thorough site evaluation is necessary. During the site evaluation, factors that need to be considered are those such as access to open water, proximity to a reef or other shoaling feature, infrastructure and security of site, and ease of station maintenance.

It is difficult to predict where a tsunami will occur and how much damage it will do. Quantifying damage prediction for affected areas requires a better understanding of tsunamigenic event origins, higher resolution bathymetry, propagation modeling in the littoral zone, and inundation mapping. Run-up and/or inundation calculations must be performed for areas most susceptible to tsunami impact (Figures 9 – 11). Mercado and McCann [1998] have begun doing this for Puerto Rico and this is already a viable product for the Pacific at the Pacific Tsunami Warning Center [*Titov, et al.*, 2001].

Sea level gauges are a part of a larger system that records, processes, and telemeters data. These stations can provide meteorological and oceanographic data to support other projects such as hurricane and storm surge monitoring and prediction, climate change monitoring, and assist in improving numerical models [*Alverson*, 2005].

These types of systems in other areas around the US are already used by harbor pilots, ship captains, the Coast Guard, recreational and commercial divers and fishermen, the surfing and sailing industry, scientists, and the general public. Therefore, to guarantee continued existence and viability, these stations must have a multi-mission purpose to garner multifaceted support because thankfully, tsunamis do not occur very often.

References

Air-Sea Monitoring Systems, A.-S. M. S. (2006), Assessment and restoration of the MACC sea-level monitoring stations travel report.

Alverson, K. (2005), Watching over the world's oceans, *Nature*, *434*, 19-20.

Baptista, M. A., et al. (2003), New study of the 1755 earthquake source based on multi-channel seismic survey data and tsunami modeling, *Natural Hazards and Earth System Sciences*, *3*, 333-340.

Bartello, P., and S. J. Thomas (1996), The cost-effectiveness of semi-Lagrangian advection, *Monthly Weather Review*, *124*, 2883-2897.

Bernard, E. N., et al. (2001), Early detection and real-time reporting of deep-ocean tsunamis, paper presented at International Tsunami Symposium, Seattle Washington.

Bilek, S. L., and T. Lay (2002), Tsunami earthquakes possibly widespread manifestations of frictional conditional stability, *Geophysical Research Letters*, *29*, 1673.

Bird, P. (2003), An updated digital model of plate boundaries, *Geochemistry, Geophysics, Geosystems*, *4*, 1027-1079.

CIAT, et al. (2005), Latin American and Caribbean Population Database, Version 3, edited, Centro Internacional de Agricultura Tropical (CIAT).

Curtis, G. D. (2001), A multi-sensor research program to improve tsunami forecasting, paper presented at International Tsunami Symposium, Seattle, Washington.

Demets, C. (1993), Earthquake slip vectors and estimates of present-day plate motions, *Journal of Geophysical Research*, *98*, 6703-6714.

Dunbar, P. (2005), National Geophysical Data Center (NGDC). National Oceanic and Atmospheric Administration (NOAA)/ National Environmental Satellite, Data, and Information Service (NESDIS), edited.

Dupont, F. (2001), Comparison of numerical methods for modeling ocean circulation in basins with irregular coasts, Dissertation thesis, McGill University, Montreal.

Fryer, G. J., and P. Watts (2000), The 1946 Unimak tsunami: Near-source modeling confirms a landslide, *EOS, Transactions, American Geophysical Union*, *81*, 748.

Fryer, G. J., et al. (2001), Source of the tsunami of 1 April 1946: A landslide in the upper Aleutian Forearc, in *Prediction of underwater landslide hazards*, edited by P. Watts, et al., Balkema, Rotterdam.

Gisler, G., et al. (2004), Two-Dimensional Simulations of Explosive Eruptions of Kick'em Jenny and other Submarine Volcanoes, paper presented at NSF Caribbean Tsunami Workshop, National Science Foundation; Los Alamos National Laboratory, Puerto Rico, 30-31 March.

Grilli, S. T., and P. Watts (2005), Tsunami generation by submarine mass failure I: Modeling, experimental validation, and sensitivity analyses, *Journal of Waterway, Port, Coastal, and Ocean Engineering*, *131*, 283-297.

Grindlay, N. R., et al. (2005), High risk of tsunami in the northern Caribbean, *EOS, Transactions, American Geophysical Union*, *86*, 121, 126.

Gusiakov, V. (2000), Tsunami travel time calculation program for the Caribbean region, edited, p. Program is on a CD, Tsunami Laboratory, Institute of Computational Mathematics and Mathematical Geophysics, Siberian Division of the Russian Academy of Sciences, Novosibirsk, Russia.

Heinrich, F., et al. (2001), Numerical simulation of the December 1997 debris avalanche in Montserrat, *Geophysical Research Letters*, *28*, 2529-2532.

Heinrich, F., et al. (1999a), Numerical modeling of a landslide generated tsunami following a potential explosion of the Montserrat Volcano, *Physics, Chemistry and Earth Sciences*, *24*, 163-168.

Heinrich, F., et al. (1998), Simulation of water waves generated by a potential debris avalanche in Montserrat, Lesser Antilles, *Geophysical Research Letters*, *25*, 3697–3700.

Heinrich, F., et al. (1999b), Modeliser un raz de maree cree par un volcan, *La Recherche*, *318*, 67-71.

Henson, J., and D. Wilson (2005), Preliminary status report on tide gauges and observing stations in the Caribbean and adjacent waters, paper presented at The Group of Experts on the Global Sea Level Observing System (GLOSS) ninth session, IOC UNESCO, Paris, France, 24 − 25 February.

Hwang, L., and A. C. Lin (1969), Experimental investigations of wave run-up under the influence of local geometry., in *Tsunamis in the Pacific Ocean*, edited by W. M. Adams, pp. 407-425, East-West Centre Press, Honolulu.

IOC-UNESCO. (2005), An Intra-Americas Sea Tsunami Warning System Project Proposal, edited, UNESCO Intergovernmental Oceanographic Commission.

Jiang, L., and P. H. LeBlond (1992), The coupling of a submarine slide and the surface waves which it generates, *Journal of Geophysical Research*, *97*, 12,731–712,744.

Kanamori, H. (1972), Mechanism of Tsunami Earthquakes, *Physics of the earth and planetary interiors 6*, 346-359.

Kato, T., et al. (2001), A new tsunami monitoring system using RTK-GPS, paper presented at International Tsunami Symposium, Seattle, Washington.

Kowalik, Z., and P. M. Whitmore (1991), An investigation of two tsunamis recorded at Adak, Alaska, *Science of Tsunami Hazards*, *9*, 67-83.

Lander, J. F., et al. (2002), A Brief History of Tsunamis in the Caribbean Sea, *Science of Tsunami Hazards*, *20*, 57.

Lander, J. F., et al. (1999), Use of tsunami histories to define the local Caribbean hazard, paper presented at International Symposium on Marine Positioning, Melbourne, Florida, December.

Mader, C. L. (2001), Modeling the 1755 Lisbon tsunami generation and propagation across the Atlantic Ocean to the Caribbean, *Science of Tsunami Hazards*, *19*, 93-98.

Martin-Kaye, P. H. A. (1969), Summary of the geology of the Lesser Antilles, *Overseas Geology & Mineral Resources*, *10*, 172-206.

Martin, P. J. (2000), A description of the Navy Coastal Ocean Model Version 1.0, 39 pp, Naval Research Laboratory, Stennis Space Center, MS.

McCann, W. R. (2004), Estimating the threat of tsunamigenic earthquakes and earthquake induced-landslide tsunami in the Caribbean, Earth Scientific Consultants, Westminster, CO.

Mercado-Irizarry, A. (2005), Professor of Physical Oceanography at the Department of Marine Sciences of the University of Puerto Rico; Coastal Hazards Specialist of the Sea Grant Program, edited, Puerto Rico.

Mercado, A., and W. McCann (1998), Numerical simulation of the 1918 Puerto Rico tsunami, *Natural Hazards*, *18*, 57-76.

Meyer, H., and J. H. Caicedo O. (1998), Evaluation of tsunami worse scenarios in the Caribbean Sea and simulation of wave weights – a TIME project activity (Oral Poster), paper presented at Okushiri Tsunami/UJNR Workshop.

Morey, S. L., et al. (2003b), Export pathways for river discharged fresh water in the northern Gulf of Mexico, *Journal of Geophysical Research*, *108*, 3303-3318.

Morey, S. L., et al. (2003a), The annual cycle of riverine influence in the eastern Gulf of Mexico basin, *Geophysical Research Letters*, *30*, 1867-1871.

Murty, T. S. (1977), Seismic Sea Waves: Tsunamis, *Bulletin of the Fisheries Research Board of Canada*, *Bull. 198*.

NGDC (2001), 2-Minute Gridded Global Relief Data (ETOPO2), edited, National Geophysical Data Center, NOAA Satellite and Information Service.

NGDC (2004), NOS EEZ Bathymetry Data, edited, National Geophysical Data Center, NOAA Satellite and Information Service.

NGDC (2005), NGDC Tsunami Database, edited, National Geophysical Data Center, NOAA Satellite and Information Service.

NOAA and USGS Fact Sheet (2005), Tsunami Detection and Warnings, edited, United States Department of Commerce, United States Department of the Interior.

O'Loughlin, K. F., and J. F. Lander (Eds.) (2003), *Caribbean Tsunamis: A 500-Year History from 1498-1998*, 263 pp., Kluwer Academic Publishers, Dordrecht.

Okada, Y. (1985), Surface deformation due to shear and tensile faults in a half space, *Bulletin of the Seismological Society of America*, *75*, 1135-1154.

Okal, E. A., et al. (2003), The deficient T waves of tsunami earthquakes, *Geophysical Journal International*, *152*, 416-432.

Pararas-Carayannis, G. (2004), Volcanic tsunami generating source mechanisms in the eastern Caribbean region, *Science of Tsunami Hazards*, *22*, 74-114.

Polet, J., and H. Kanamori (2000), Shallow subduction zone earthquakes and their tsunamigenic potential, *Geophysical Journal International*, *142*, 684-702.

Reid, H. F., and S. Taber (1919), The Porto Rico earthquake of 1918, House of Representatives, 66th Congress, 1st Session, Washington D.C., United States.

Rueda, F. J., and S. G. Schladow (2002), Quantitative comparison of models for barotropic response of homogeneous basins, *Journal of Hydraulic Engineering*, *128*, 201.

Shuto, N. (1991), Numerical simulations of tsunamis – its present and near future, *Natural Hazards*, *4*, 171-191.

Sigurdsson, H. R. (1996), Volcanic Tsunamis, Summary Report for the UNESCO IOC IOCARIBE Tsunami Warning Workshop, UNESCO IOC IOCARIBE, Paris.

Smith, M. S., and J. B. Shepherd (1993), Preliminary investigation of the tsunami hazard of Kick'em Jenny submarine Volcano, *Natural Hazards*, *7*, 257-277.

Smith, M. S., and J. B. Shepherd (1994), Explosive submarine eruptions of Kick'em Jenny volcano: Preliminary investigations of the potential tsunami hazard in the eastern Caribbean region, paper presented at Caribbean Conference on Natural Hazards; volcanoes, earthquakes, windstorms, floods, St. Ann's Trinidad and Tobago, October 11-15.

Smith, M. S., and J. B. Shepherd (1995), Potential Cauchy-Poisson waves generated by submarine eruptions of Kick 'em Jenny volcano, *Natural Hazards*, *11*, 75-94.

Sykes, L. R., et al. (1982), Motion of Caribbean plate during the last 7 million years and implications for earlier cenozonic movements, *Journal of Geophysical Research*, *70*, 5065-5074.

ten Brink, U. S., et al. (2004), New seafloor map of the Puerto Rico Trench helps assess earthquake and tsunami hazards, *EOS, Transactions, American Geophysical Union*, *85*, 349-360.

Titov, V. V., et al. (2001), Project SIFT (Short-term Inundation Forecasting for Tsunamis), paper presented at International Tsunami Symposium, Seattle, Washington.

Todorovska, M. I., and M. D. Trifunac (2001), Generation of tsunamis by slowly spreading uplift of the sea floor, *Soil Dynamics and Earthquake Engineering*, *21*, 151-167.

von Hillebrandt-Andrade, C. (2006), Puerto Rico Tsunami Ready Tide Gauge Network; Puerto Rico Seismic Network, edited.

von Huene, R., et al. (1989), A large tsunamigenic landslide and debris flow along the Peru trench, *Journal of Geophysical Research*, *94*, 1703-1714.

Watts, P., and S. T. Grilli (2004 (Submitted)), Tsunami generation by submarine mass faliure: Part I wavemaker models, *J. Waterway, Port, Coastal, and Ocean Engineering*.

Watts, P., et al. (2003), Landslide tsunami case studies using a Boussinesq model and a fully nonlinear tsunami generation model, *Natural Hazards and Earth System Sciences*, *3*, 391-402.

Weissert, T. P. (1990), Tsunami travel time charts for the Caribbean, *Science of Tsunami Hazards*, *8*, 67-78.

Whitmore, P. M. (2003), Tsunami amplitude prediction during events: A test based on previous tsunamis, *Science of Tsunami Hazards*, *21*, 135-143.

Woods Hole, O. I. (2005), Major Caribbean earthquakes and tsunamis a real risk, edited, SCI/TECH. YubaNet.com.

Zahibo, N., et al. (2003b), Estimation of far-field tsunami potential for the Caribbean coast based on numerical simulation, *Science of Tsunami Hazards*, *21*, 202-222.

Zahibo, N., et al. (2003a), The 1867 Virgin Island tsunami: observations and modeling, *Oceanologica Acta*, *26*, 609-621.

Bibliography

Anderson, J. (1784), An account of Morne Garou, a mountain in the island of St. Vincent with a description of the volcano on its summit, *Philosophical Transactions of the Royal Society*, *125*, 32.

Anderson, T. (1903), Recent volcanic eruptions in the West Indies, *The Geographical Journal*.

Anderson, T. (1908), Report on the eruptions of the Soufrière in St. Vincent in 1902, and on a visit to Montagne Pelèe in Martinique - The changes in the district and the subsequent history of the volcanoes, *Philosophical Transactions of the Royal Society*, *Series A-208 (Part II)*, 275-352.

Anderson, T., and S. J. Flett (1903), Report on the eruption of the Soufrière of St. Vincent in 1902 and on a visit to Montagne Pelèe in Martinique, *Royal Society Philosophical Transactions*, *Series A-200 (Part I)*, 353-553.

Carey, S. N., and H. R. Sigurdsson (1978), Deep-sea evidence for distribution of tephra from the mixed magma eruption of the Soufrière on St. Vincent, 1902: Ash turbidites and air fall, *Geology*, *6*, 271-274.

Choi, B. H., et al. (2003), Simulation of the trans-oceanic tsunami propagation due to the 1883 Krakatau volcanic eruption, *Natural Hazards and Earth System Sciences*, *3*, 321-332.

Earthquake Research Committee, (2002), Seismic activity in Japan -- regional perspectives on the characteristics of destructive earthquakes, Headquarters for Earthquake Research Promotion, Japan.

Feuillet, N., et al. (2002), Arc parallel extension and localization of volcanic complexes in Guadeloupe, Lesser Antilles, *Journal of Geophysical Research*, *107*, 2331.

Hooper, D. M., and G. S. Mattioli (2001), Kinematic modeling of pyroclastic flows produced by gravitational dome collapse at Soufriere Hills Volcano, Montserrat, *Natural Hazards*, *23*, 65-86.

Mader, C. L. (2001), Modeling the La Palma Landslide Tsunami, *Science of Tsunami Hazards*, *19*, 150-170.

Mercado, A., and W. McCann (2001), Evaluation of the tsunami hazard for Eastern Hispaniola and Western Puerto Rico in the Caribbean Sea Region (Oral Poster), paper presented at International Tsunami Symposium, Seattle, Washington.

Pelinovsky, E., et al. (2004), Tsunami generated by the volcano eruption on July 12-13, 2003 at Montserrat, Lesser Antilles, *Science of Tsunami Hazards*, *22*, 44-57.

Perret, F. A. (1937), The eruption of Mt. Pelee, 1929-1932, *Carnegie Institute of Washington Publication*, *458*, 126.

ten Brink, U. S., et al. (2002), The nature of the crust under Cayman Trough from gravity, *Marine and Petroleum Geology*, *19*, 971-987.

USGS (1999), Seismic and Tsunami Hazard in Puerto Rico and the Virgin Islands, paper presented at USGS Workshop, Colegio de Ingenieros y Agrimensores, San Juan, 23-24 March.

Yalciner, A. C. (2004), Modeling of tsunamis in the eastern Mediterranean and comparison with Caribbean (Oral Poster), paper presented at NSF Caribbean Tsunami Workshop, National Science Foundation; Los Alamos National Laboratory, Puerto Rico, 30-31 March.

Appendices

APPENDIX A: A NOTE ON DRY CELL ISSUES AND BATHYMETRY ALTERATIONS

The NCOM is running on a 2 arc-min resolution grid with one depth averaged vertical grid cell. Some of the historical tsunami simulations will cause all of the water in a shallow grid cell to slosh out leaving the cell dry. The NCOM will crash when this occurs because it is not able to solve the equations described in Methods ("Modeling").

To solve this problem, the model is configured to modify the ETOPO2 bathymetry dataset to eliminate cells that are shallower than 2 m. This converts cells less than 2 m to 2 m. However, this is not sufficient for some of the simulations and the ETOPO2 bathymetry is changed to be no shallower than 4 m. It is assumed that differences observed between a 2 and 4 m modification are equivalent to differences between a 2 m alteration and no adjustment. This assumption is valid because the number of cells affected from each modification is equivalent.

Wave propagation, group speed, and therefore travel time are dependant on water depth. Changing the bathymetry has the possibility of affecting the results of the simulation. In order to determine if these changes are significant, the 1918 tsunami originating off of Puerto Rico is simulated with both a 2 and 4 m bathymetry adjustment and the same locations listed in Appendix B (see Table B1) are evaluated. These experiments are run for 8 hr. A surface elevation time series is plotted for each location and the data from one experiment is regressed against the other. Two locations are specifically discussed.

The linear regression of surface elevation time series' at Punto Higuero results in a correlation coefficient of 0.9779. The Santo Domingo site has coefficient of 0.9942 up to record 171 (approximately 2 hr), but this value declines to 0.8965 once the full 8 hr (641 records) is used. When comparing the 2 and 4 m simulations to each other, the majority of the sites (see Table B1) have very similar amplitudes for approximately the first 100 (74.25 min) to 200 (149.25 min) records but diverge thereafter. Based on the correlation and amplitude similarities between each simulation for all of the sites, the difference between bathymetry filters is not significant.

APPENDIX B: INITIAL CONDITION AND NCOM PARAMETER OPTIONS EXPERIMENTS

Introduction

Sensitivity tests are run to identify initial wave amplitude and e-folding radius, bottom roughness coefficient, model time step, surface field output interval, and total run time. These parameters are tested using the 1918 tsunami originating off of Puerto Rico. The final results of these tests are discussed in the main body of the manuscript under Methods ("Modeling"). These choices are used to simulate all 42 historical tsunamis.

Methods

After each 1918 simulation a time series is extracted for 7 locations around Puerto Rico, the United States Virgin Islands, and the Dominican Republic (Table B1). The grid resolution and bathymetry data used for these tests is identical to that used in the main study. Table B2 lists the initial condition and model parameter experiment values tested. The e-folding radius, bottom roughness coefficient, and total run time values are finalized in later trials. These later experiments use an initial amplitude, model time step, and a surface field output interval of 4 m, 7.5 sec, and 45 sec respectively. The bottom roughness experiment uses all 10,623 CGP's for analysis.

A surface elevation time series is plotted for each location and the data from one experiment is regressed against the other. A linear regression correlation coefficient of 1 should result if the change in the parameter(s) does not affect the model output. This result means that the NCOM is not sensitive to those changes.

Table B1 – Time series analysis locations. The latitude and longitude is rounded to the nearest CGP and the site elevation is taken from the ETOPO2 bathymetry.

Name	Long (E)	Lat (N)	Site elev. (m)
Caja de Muertos, PR	-66.50	18.60	-885
Isabella, PR	-67.00	18.53	-301
Punta Higuero, PR	-67.23	18.40	-131
Rio Grande, PR	-65.73	18.47	-44
Tortola, USVI	-64.60	18.50	-18
Krum Bay, USVI	-64.90	18.37	-1
Santo Domingo (Rio Ozama), DR	-69.87	18.47	-13

Table B2 – Values used in sensitivity experiments 1-10.

Exp #	Initial amp (m)	Integration time step (s)	Surface field output interval (min)	[surface field output interval (s)] / [time step (s)]
1	2	12.00	6.00	30.00
2	4	12.00	6.00	30.00
3	4	12.00	3.00	15.00
4	4	12.00	1.50	7.50
5	4	31.00	1.50	2.90
6	4	6.00	1.50	15.00

APPENDIX B (Continued)

Table B2 (Continued)

Exp #	Initial amp (m)	Integration time step (s)	Surface field output interval (min)	[surface field output interval (s)] / [time step (s)]
7	4	7.50	1.50	12.00
8	4	15.00	1.50	6.00
9	4	3.75	1.50	24.00
10	4	7.50	0.75	6.00

Results and Discussion

Surface field output interval

The parameter that dictates temporal resolution of a surface elevation time series is the surface field output interval. The limiting factor for this interval is the amount of space available for data storage. Decreasing the surface field output interval proportionally increases the memory required to store the output data. Temporal resolution is important to identify the first peak or trough reaching the CGP.

When the output interval is 6 or 3 min the surface elevation time series resolution is not high enough to discern the exact moment of impact. Based on the Rio Grande, PR and Caja de Muertos, PR locations, the output interval needs to be 1.5 min. However, the location closest to the tsunami origin, Punta Higuero, has a travel time of 1.5 min faster in experiment 9 than in experiments 7 and 8. To resolve this discrepancy, the surface field output interval was decreased from 1.5 min in experiment 9 to 45 sec in experiment 10. Experiment 10 uses the same integration time step as experiment 7 and a surface field output interval of 45sec. Two locations had the same travel time, one location was 45 sec slower and the remaining 4 locations were 45 sec faster. This discrepancy is within the accuracy of the model output considering its dependence on the initial conditions and bathymetry.

It should be noted that the integration time step and surface field output interval must be a multiple of each other in order to compare the effect of changing the integration time step. The data from each surface field output interval will be interpolated by the NCOM if the integration time step is not a multiple of the surface field output interval (see Table B2). Therefore, experiments 4 and 5 data are not used.

Integration time step

An integration time step of 12 sec will run a simulation at 50% real time. The limiting factor for the time step is the amount of time required to run the simulation. This must be considered due to the time constraints of this project. Increasing the model time step proportionally reduces the processing time.

Based on the results from experiments 4 through 8, an integration time step of at least 7.5 sec is necessary. The model results have significant differences between a 24 and 6 sec and between a 6 and 12 sec integration time step. The differences between integration time steps of 7.5 sec (experiment 7) and 15 sec (experiment 8) are not as evident. The travel time calculated to all of the locations (see Table B1) in experiment 7

is the same as in experiment 8. However, the phases of the surface elevation time series at the sample locations produced by experiments 7 and 8 are not in agreement after initial impact and wave magnitudes are never in agreement. When comparing the locations, the wave height difference between an integration time step of 7.5 and 15 sec decreases with distance from origin but this relationship is not linear. There is a stronger correlation between experiments 7 and 8 with decreasing water depth after normalizing it with either distance from origin or travel time. The average linear regression correlation coefficient between the two experiments for all locations is just above 0.5. This correlation is not sufficient to conclude that an integration time step of 7.5 sec yields the same results as an integration time step of 15sec. Therefore, an integration time step of 15 sec is too long. Experiment 9 tests an integration time step of 3.75 sec to determine if an integration time step of 7.5 sec is sufficient.

The comparison between experiments 7 and 9 (7 and 3.75 sec) gives similar results to the comparison of 7 and 8 (7 and 15 sec). The general trend of increased correlation with distance away from the origin and increasing travel time is stronger. For all but one location, Punta Higuero, PR, the travel time is the same for experiments 7, 8, and 9. The variation between experiments 7 and 9 is acceptable and a time step 7.5 sec is used.

For an average tsunami celerity in the Caribbean of approximately 450 kph, roughly 3.5 time integration steps pass as a tsunami moves from one grid point to another. Almost 2 time steps pass if the celerity is 800 kph (a more typical speed in deeper water). In either case, the CFL condition is met as long as the celerity is less than 1584 kph (Mach 1.29) which is only possible if the ocean is ~ 255 km deep. The CFL condition is always be satisfied. CFL is described in more detail in the main body of the manuscript under Methods ("Modeling").

Initial amplitude and e-folding radius

Differences in initial amplitude and e-folding radius will change which locations are impacted. This is because a larger initial amplitude and/or e-folding radius impart more energy to the ocean and the resulting tsunami travels farther over a shelf or other shoaling feature. The travel time and phase results appear to be the same when the initial amplitude is either 2 or 4 m. Based on this and previous works, an initial amplitude of 4 m is an accurate representation of the tsunamigenic events simulated in this study [*Mercado and McCann*, 1998; *Meyer and Caicedo O.*, 1998; *Zahibo, et al.*, 2003b; *Zahibo, et al.*, 2003a].

The travel time is affected by a change in e-folding radius from 10 to 40 km. The travel time is affected in the short term since the origin with the larger e-folding radius is closer to a coastline by 30 km. This travel time difference is on the order of 6 – 10 min. Travel time should not be affected in the long term because celerity is only a function of bathymetry and gravity. In addition, an e-folding radius of 40 km produces a larger amplitude wave train, creating dry cells. An e-folding radius of 10 km is used.

APPENDIX B (Continued)

Seafloor roughness

The travel time is also affected by a difference in seafloor roughness. Two coefficients, 0.01 and 0.003, are tested. Out of 10,623 coastal grid points analyzed, approximately 2% have a difference in travel time. The average difference is 10 min with a maximum and minimum difference of 78 and 0.75 min, respectively. Of the points with a different travel time (2%), approximately 43% of them have a faster travel time associated with a roughness coefficient of 0.01. This may be to due to wave interactions and shore reflections. Baptista et al. [2003] showed that travel time and wave heights change proportionally with seafloor roughness. A more common coefficient is 0.003 and is used in this study [*Mercado and McCann*, 1998].

Total run time

Although these experiments are run for 8 hr it is only necessary to run a simulation for 6 hr. This is determined by observing propagation throughout the IAS via animations created from the NCOM output. More information regarding the physical parameters and numerical options used is available upon request of the authors.

APPENDIX C: TRAVEL TIME POST PROCESSING EXPERIMENTS

Introduction

Using the initial conditions and NCOM parameters identified in the sub-study described in Appendix B, the 1918 tsunami generated off of Puerto Rico is simulated to develop a travel time post processing method. A surface elevation time series is extracted for each location listed in Appendix B (see Table B1). These time series' are used to determine a signal to noise threshold and a method for peak and trough identification.

The travel time to each CGP is defined as the time corresponding to the first peak or trough. It is easy to manually distinguish between noise and the tsunami signal (Figure C1). However, in order to automate the travel time calculation process, a threshold criterion is necessary. The hypothesis is that the arrival of a tsunami should be associated with a rate of change greater than some value found in the numerical noise. The requirement is to determine a threshold that is surpassed after the last peak or trough in the noise but before the first peak or trough in the tsunami signal.

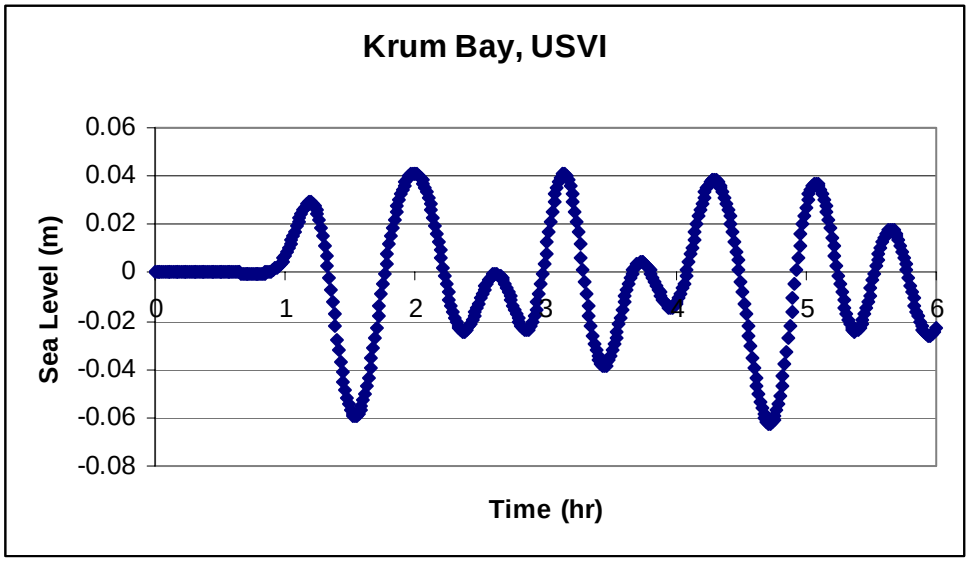

Figure C1 – Surface elevation time series at Krum Bay, USVI resulting from the 1918 Puerto Rico tsunami. It is important to note that, as explained in the main body of this manuscript, the elevation is not necessarily representative of realistic amplitude.

Methods and Discussion

The time series output is used to develop and test both the threshold and peak/trough identification equations. The 9 locations used in the experiment are those seen in table B1 as well as two other locations along a coastline where an impact is not expected. This expectation is visually derived from animation created from the NCOM output.

Data is recorded at every grid point in the model whether a tsunami signal is present or not. Since the amplitudes calculated by the NCOM may not be accurate, small amplitude signals (less than 0.25 m) are considered for a tsunami signal. Therefore, relative changes must be used identify the presence of a tsunami.

APPENDIX C (Continued)

Using the hypothesis noted in the introduction a simple rate of change formula is tested (Equation C1).

$$H_n - H_{n-1} \tag{C1}$$

where,
H = sea level and n = record number

This equation describes the elevation at the time or record in question minus the record prior to it. A tsunami signal is considered present if the resulting value is greater than some number yet to be identified. This number or threshold is derived by applying the equation to a time series where the tsunami signal can be readily observed as in figure C1. This formula acts as a criterion to be met before a second formula is applied to identify the peak or trough. However, equation C1 discriminates between increasing and decreasing sea level. To eliminate sign bias this equation is squared (Equation C2).

$$\left(H_n - H_{n-1}\right)^2 \tag{C2}$$

Equation C2 fails to consistently distinguish the beginning of the tsunami signal from the noise and at some locations produces larger values in the noise than at the beginning of the tsunami signal. Therefore, no limiting value will work and another solution is required.

Rate of change is defined here, as a change in elevation over a constant time period. The next hypothesis tests if an increased time period yields smaller values in the noise than at the beginning of the tsunami signal. The next equation tested is

$$\left(H_n - H_{n-2}\right)^2 \tag{C3}$$

This equation does not produce higher values in the noise than at the beginning of the tsunami signal and thus is acceptable. The next step is to determine what the threshold value should be. Equation C3 is applied to the test locations time series' and since the time at the first peak is already established for these locations, a value that marks the beginning of the tsunami signal is selected. The result of this iterative process is a value of 0.00001 (Equation C4). This consistently marks the beginning of the tsunami signal when it is present and does not when no signal is present. Figure C2 is an example of a location that did not record a tsunami signal.

$$\left(H_n - H_{n-2}\right)^2 > 0.00001 \tag{C4}$$

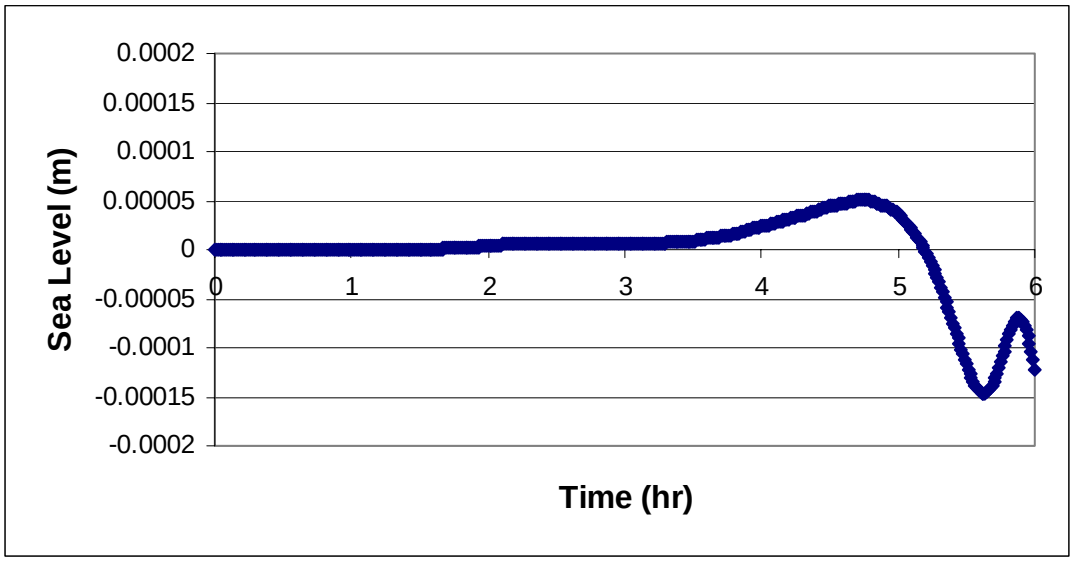

Figure C2 - Surface elevation time series at a generic point resulting from the 1918 Puerto Rico tsunami. Note that a tsunami signal is not present and a tsunami would not be considered to have impacted this location.

Once the threshold is reached, another equation determines the exact record or time at the peak or trough. Equation C5,

$$H_n - H_{n-1} \tag{C5}$$

results in a positive number if the sea level is going up and a negative number if it is going down. The same is true for equation C6,

$$H_{n+1} - H_n \tag{C6}$$

Like sign numbers divided will always yield a positive number and opposite sign numbers divided will always yield a negative number. As the signal continues in the same direction the result to equation C7 will be positive, but if it changes direction over 3 records the result will be negative. Therefore, if equation C7 is satisfied it can be said that a peak or trough is present at record n.

$$\frac{H_{n+1} - H_n}{H_n - H_{n-1}} > 0 \tag{C7}$$

This only holds true if the temporal resolution is high enough to eliminate the possibility of two data points having the exact same elevation at the same peak or trough. Based on the 1918 simulation and locations tested, the temporal resolution (45 sec) is high enough. However, during the post processing of the NCOM data, it was discovered that in some cases this resolution is not high enough. Post processing consists of evaluating a time series at 10,623 points for 42 simulations, to determine the first peak or trough by applying the criteria shown in equations C4 and C7. Out of these 446,166 time series, 5 had two points at the same peak, and 2 had two points in the first peak. When a time series has two points at the same peak or trough, equation C7 will result in a divide by zero error. The program written for post processing notes this error and returns the point at which this occurs. This is therefore easily corrected by manually analyzing the surface elevation time series for those locations and selecting the first peak or trough value.

APPENDIX D: ISOCHRON / NCOM TTT COMPARISON TESTS

Introduction

The isochrones are developed using an average tsunami celerity of approximately 450 kph (Figure D1). This value is calculated using historical observations, the NCOM results, Mercado and McCann [1998] results, and the average depth of the Caribbean.

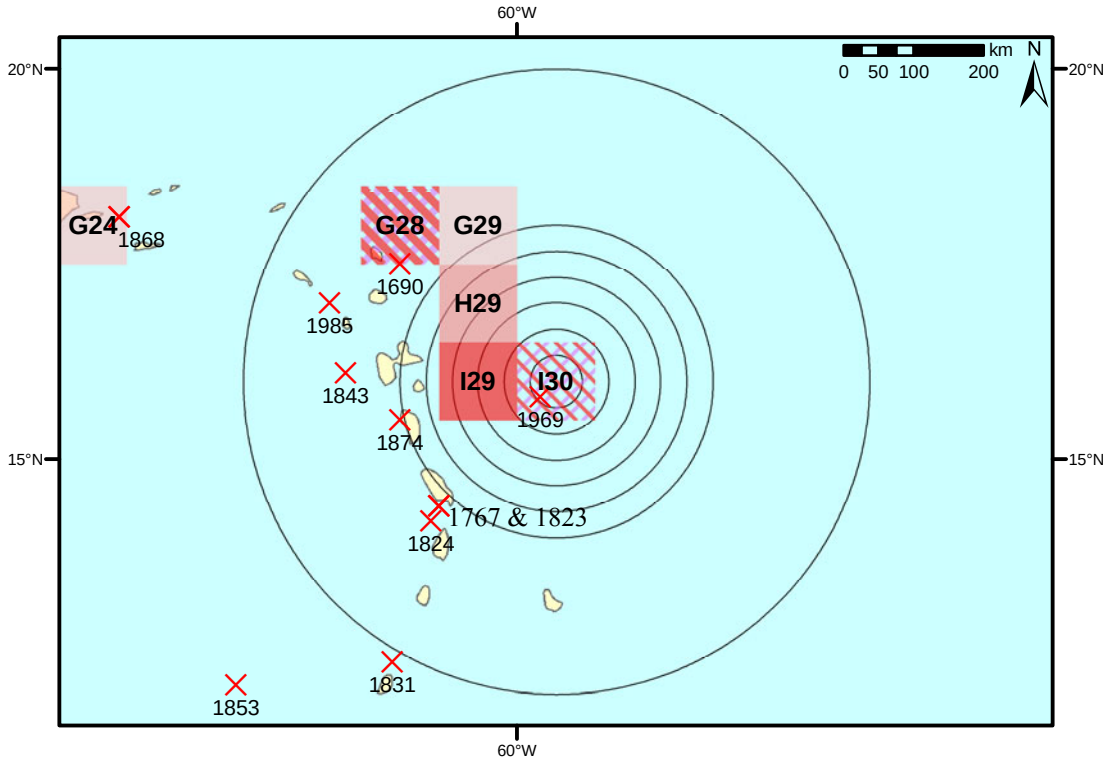

Figure D1 - Sector I30 isochrones. The isochrones start at 5 min and increase in 5 min intervals out to 30 min. The largest isochron is 60 min. Note the 1767 and 1823 tsunamis have the same origin coordinates.

Methods

Out of the 15 relatively higher risk sectors (see Figure 8 in Methods – Sea Level Gauge Location Determination), 10 encompass an area where at least 1 historical tsunami originated. Travel time from the tsunami origins within 9 of the sectors is compared to travel time calculated from the center of the corresponding sectors. For example, in figure D1, travel time estimates from the 1969 tsunami are compared to travel time estimates from the center of sector I30. Note that the tsunami origins being compared are not in the same location. In the event more than 1 tsunami origin is with in a sector the tsunami origin closest to the center of the sector is used. Within these 9 sectors, 37 locations are not protected based on the isochron analysis. These 9 sectors are used to compare the NCOM and isochron warning times. It is not possible to estimate NCOM travel time to some of the locations selected for a sea level gauge due to the limitations of ETOPO2 bathymetry. In these cases the point is adjusted to the nearest CGP.

APPENDIX D (Continued)

Results and Discussion

In general, the NCOM travel times are slower than the isochron travel times but they are also equal to and faster than the isochron times. The difference between the isochron and NCOM travel times is larger at locations close to the center of a sector and at those that have deep water close to the coast. This difference is most significant for population centers close to or at the 30 min warning time criteria.

The mean travel time difference, where the NCOM travel time is shorter than the isochron travel time, is 16.5 ± 19.45 min. The status of 4 locations could be changed to warned if this is considered a significant difference. However, as stated above, the NCOM tsunamis used for comparison originate in slightly different locations and warning time estimates must be conservative. Changing the status of a few locations based on this sub-study will eliminate some conservation.

APPENDIX E: Travel Time Verification Study

Introduction

Travel time is defined as the record or time corresponding to the first peak or trough seen at a location. A simulation of the 1918 tsunami generated off of Puerto Rico is used for verification. Although the surface elevation time series' shown here only display the first 75 min, this simulation was run for 8 hr. Reid and Taber [1919] report travel times to a variety of locations, but only Mayagüez, Aguadilla, and Boqueron are discussed here for the sake of brevity. These locations are used to compare results from this study to results from Mercado and McCann [1998] and historical observations from Reid and Taber [1919]. Travel times reported from both studies are in general agreement with those calculated here.

Results and Discussion

Aguadilla

The Mercado and McCann [1998] travel time to Aquadilla is very similar to that found in this study. Both works estimate a travel time of ~ 6 min (Figure 1E). Reid and Taber [1919] report a travel time from different observers of 4 – 7 min. Mercado and McCann [1998] show a 3 m trough after the initial crest (0.7 m) and the second peak at twice the amplitude of the first. Although there are phase and wave height differences, the relative amplitude of the peaks and troughs shown here are also similar to those found in Mercado and McCann [1998].

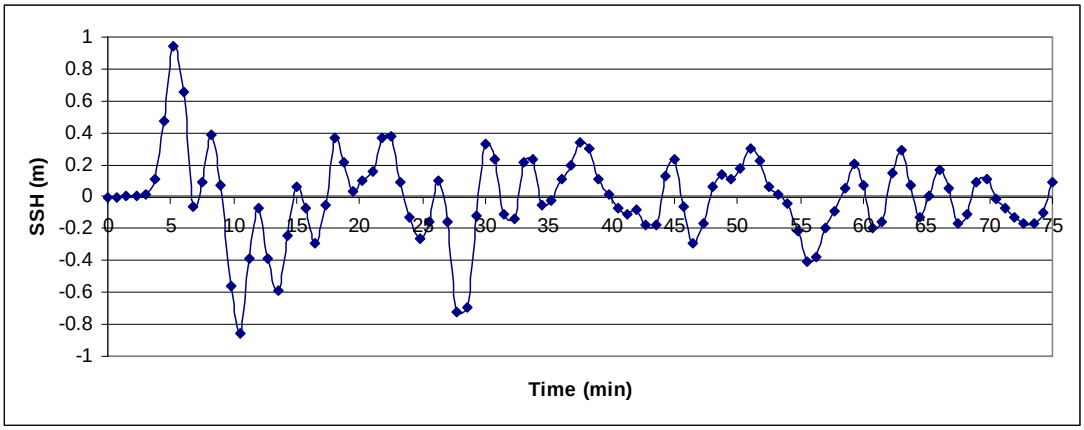

Figure E1 – Sea level time series at Aguadilla resulting from the 1918 Puerto Rico Tsunami.

Mayagüez

This study as well as Reid and Taber [1919] show a travel time of approximately 23 min to Mayagüez. Mercado and McCann [1998] show large trough arriving first at 23 min and the following crest at 30 min. The amplitude seen here (Figure 2E) is smaller than that seen in the Mercado and McCann [1998] time series (~ 0.8 m). Interestingly, another time series from this study at a grid point just east of Mayagüez, in the bay of Mayagüez, has a maximum amplitude of ~ 0.9 m (Figure 3E). This time series looks very similar to that shown in Mercado and McCann [1998]. The offshore grid point may

be more appropriate to use for comparison because here, the behavior of the wave closer to shore may not be properly resolved due to the bathymetry and/or model resolution.

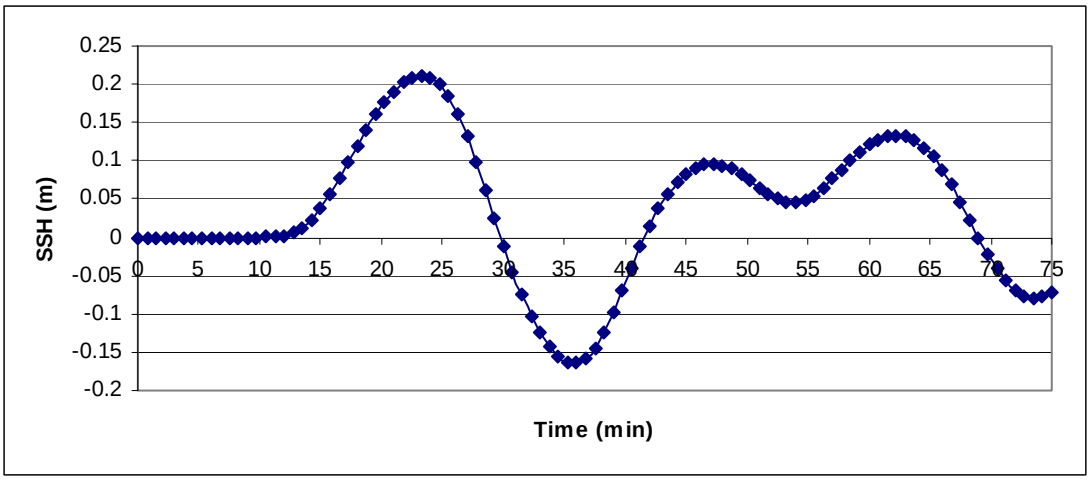

Figure E2 – Sea level time series at Mayagüez resulting from the 1918 Puerto Rico Tsunami.

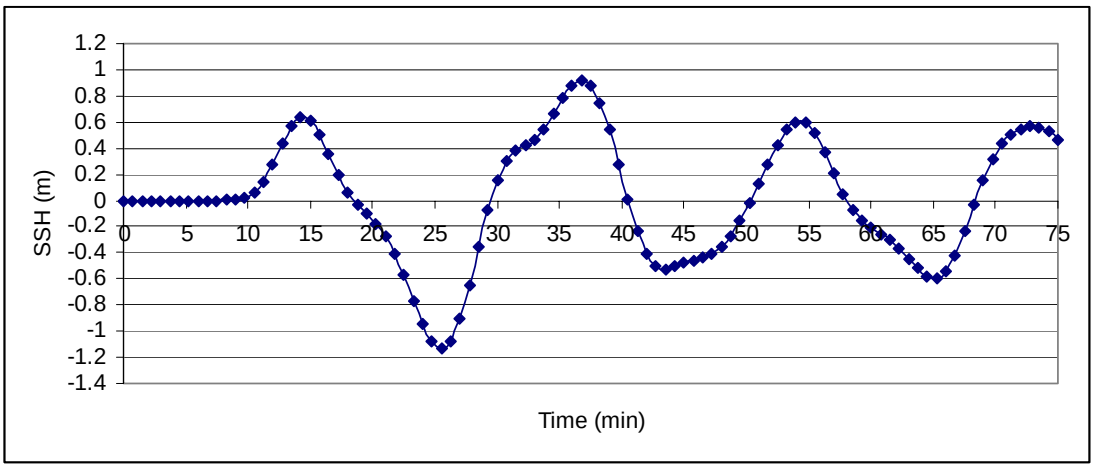

Figure E3 – Sea level time series just east of Mayagüez, in the bay of Mayagüez resulting from the 1918 Puerto Rico Tsunami.

Boqueron

Reid and Taber [1919] report a travel time of 45 min, the Mercado and McCann [1998] time series shows a travel time of approximately 47 min to the first trough (arrives first), and this study finds a travel time of approximately 45 min to the first crest (Figure 4E). The phase difference between this work and Mercado and McCann [1998] seen at Mayagüez is present here as well. In addition, the Mercado and McCann [1998] temporal resolution appears to be higher than that used in this study (45 sec) which may also effect

the differences in results. The amplitude seen here (Figure 4E) is smaller than that published in Mercado and McCann [1998] (0.9 m).

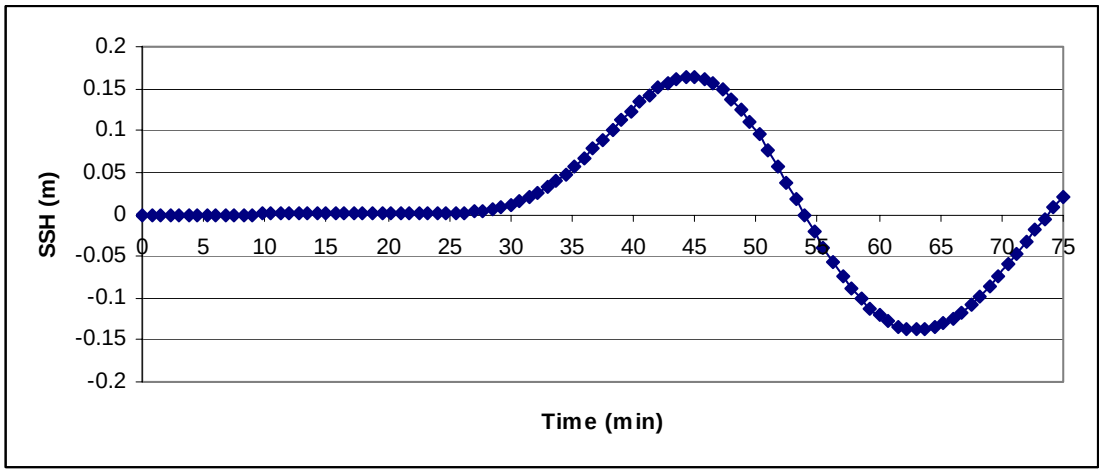

Figure E4 – Sea level time series at Boqueron resulting from the 1918 Puerto Rico Tsunami.

Conclusion

Reasons for the discrepancy with Mercado and McCann [1998] may be because they use a higher bathymetric and horizontal grid resolution, more accurate bathymetry, and run-up capability. They use a 3 arc-second grid resolution and this study uses a 2 arc-min grid resolution. In addition, the location and shape of the initial wave is also different. They generate the tsunami along a multi-segment fault line whereas it is considered a point source here.

Run up and/or local bathymetric effects are not considered and the resulting wave amplitudes are therefore, in some cases, smaller. This can be taken into account by adding a multiplier to all of the wave heights but this requires further analysis since the local bathymetric effects can also decrease wave height. In general, based on comparisons with Reid and Taber's [1919] historical observations and the Mercado and McCann [1998] modeling, this study's reported relative amplitudes and travel times appear to be accurate.